Leaching characteristics and mechanism of the synthetic calcium-aluminate slags for alumina recovery

Azof, Fabian Imanasa; Yang, Yongxiang; Panias, Dimitrios; Kolbeinsen, Leiv; Safarian, Jafar

DOI
10.1016/j.hydromet.2019.03.006

Publication date
2019

Document Version
Final published version

Published in
Hydrometallurgy

Hydrometallurgy 185 (2019) 273–290

Contents lists available at ScienceDirect

Hydrometallurgy

journal homepage: www.elsevier.com/locate/hydromet

Leaching characteristics and mechanism of the synthetic calcium-aluminate slags for alumina recovery

Fabian Imanasa Azof[a,*], Yongxiang Yang[a,b], Dimitrios Panias[c], Leiv Kolbeinsen[a], Jafar Safarian[a]

[a] Department of Materials Science and Engineering, Norwegian University of Science and Technology (NTNU), Trondheim, Norway
[b] Department of Materials Science and Engineering, Delft University of Technology, Delft, the Netherlands
[c] School of Mining and Metallurgical Engineering, National Technical University of Athens (NTUA), Athens, Greece

ARTICLE INFO

Keywords:
Leaching characteristics
Leaching mechanism
Calcium-aluminate slags
Alumina
$CaO-Al_2O_3$ system

ABSTRACT

The leaching characteristics and mechanism of synthetic $CaO-Al_2O_3$ slags in alkaline solution at atmospheric pressure have been studied. The purpose of the study is to have a better understanding of the leaching part of the Pedersen process, as an alternative to the Bayer process for alumina production. The crystalline slags containing $CaAl_2O_4$, $Ca_3Al_2O_6$, $CaAl_4O_7$, and $Ca_{12}Al_{14}O_{33}$ phases, and leaching residues (predominantly $CaCO_3$) are characterized by X-ray Diffraction and semi-quantitative analysis. Of the leaching characteristics in a solution containing 120 g/L Na_2CO_3, the slag with the highest amount of $Ca_{12}Al_{14}O_{33}$ phase is the most leachable one in the $CaO-Al_2O_3$ system with about 95% of alumina extraction. The leaching extent is confirmed employing Inductively Coupled Plasma-High Resolution-Mass Spectrometer (ICP-HR-MS) analysis, and it decreases by 0.4% for every percent of the bayerite ($Al(OH)_3$) formation during the leaching. The less stable form of $CaCO_3$, i.e., vaterite, is formed over the leached slag particles that consist 33–49 wt% CaO, while $Ca_3Al_2(OH)_{12}$ (tricalcium alumina hydrate) precipitated at relatively low concentrations (< 6 wt%) in all residue. The non-bridging oxygen (NBO) over tetrahedral structure (T) index shows that the atomic structure may affect the leaching extent of the slags, the lower NBO/T index of the phase is the more difficult for the phase to leach or depolymerize. However, the $Ca_{12}Al_{14}O_{33}$ phase is an exception case where it has "free" O-ions at the center of the cage structure, which makes it easily depolymerize, therefore, the NBO/T index for the $Ca_{12}Al_{14}O_{33}$ phase becomes irrelevant. Furthermore, the morphology and size evolution of the obtained residue measured with laser particle analyzer indicates the agglomeration behavior of the residue particles during the leaching process.

1. Introduction

In alumina production by the Bayer process, the digestion of bauxite is one of the most energy consuming steps compared to the other parts (Gu et al., 2007; Mach, 2012). The digestion effectiveness of bauxite in this process mainly depends on its mineralogy (e.g., gibbsite, boehmite, or diaspore) knowing that different Al_2O_3-containing minerals require different digestion conditions (Meyer, 2004). Monohydrates (γ-AlOOH and α-AlOOH) are less reactive than the trihydrates (γ-$Al(OH)_3$), which needs a higher temperature and alkali concentration for their digestion (Alex et al., 2013). Nevertheless, all three minerals need considerably high pressure and temperature to yield the metallurgical grade of alumina. It is also known that the pre-desilication process at elevated temperature (Smith, 2009) and the bauxite residue (red mud) of this process have severe problems with the environment (Azof et al., 2018a; Safarian, 2018; Safarian and Kolbeinsen, 2016a, 2016b; Sellaeg et al., 2017), which need attentive regulation concerning its disposal and storage (Dentoni et al., 2014; World Aluminum, 2015).

Harald Pedersen (1927) had proven that it is viable to yield alumina at low pressure and temperature-leaching of calcium-aluminate slags that is produced from smelting-reduction of bauxite. The process does not produce red mud as the iron oxides of the bauxite is 99.9% reduced during the smelting (Azof et al., 2018b). Furthermore, the CO_2 gas produced from the smelting-reduction process can be utilized in its later process (precipitation), and the sodium carbonate used in the leaching treatment could be recovered from the leachate during the precipitation (see Fig. 1). Therefore, the Pedersen process can be a good alternative for alumina recovery with lower environmental impact than the Bayer process.

Some studies concerning the leachability of calcium aluminate

* Corresponding author at: Department of Materials Science and Engineering, Norwegian University of Science and Technology (NTNU), Bergbygget E-133, Trondheim N-7491, Norway.
E-mail addresses: fabian.i.azof@ntnu.no (F.I. Azof), y.yang@tudelft.nl (Y. Yang), panias@metal.ntua.gr (D. Panias), leiv.kolbeinsen@ntnu.no (L. Kolbeinsen), jafar.safarian@ntnu.no (J. Safarian).

https://doi.org/10.1016/j.hydromet.2019.03.006
Received 30 November 2018; Received in revised form 10 March 2019; Accepted 17 March 2019
Available online 19 March 2019

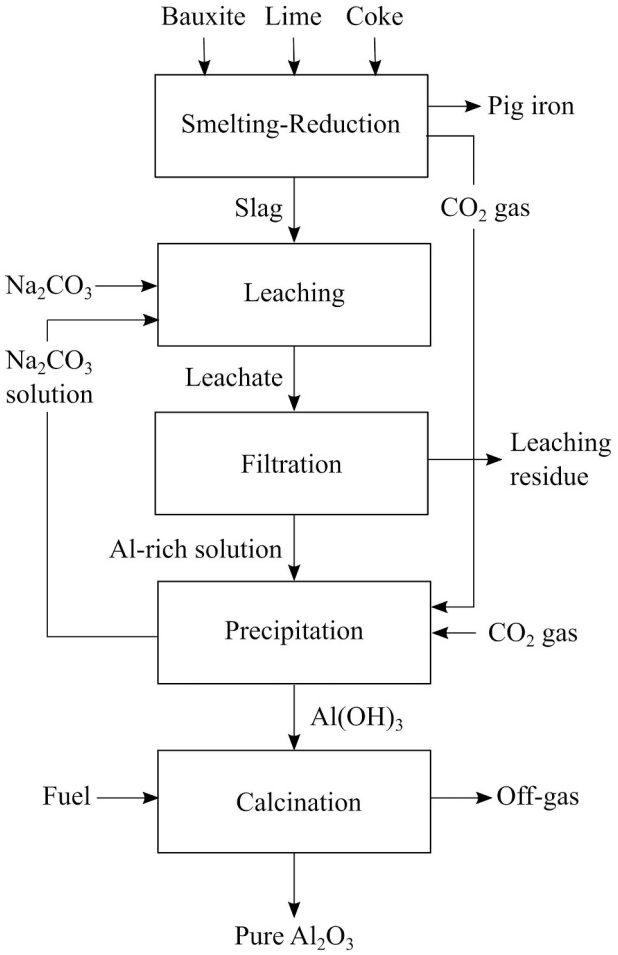

Fig. 1. Simplified flowsheet for material flow in the Pedersen Process.

phases in a $CaO\text{-}Al_2O_3$ binary system have been done in the past. Lundquist and Leitch (1963a), Lundquist and Leitch, 1963b, Lundquist and Leitch, 1964) studied the alumina leachability of $CaAl_2O_4$ (CA), $Ca_{12}Al_{14}O_{33}$ ($C_{12}A_7$) and $Ca_3Al_2O_6$ (C_3A) phases that was produced from the lime-soda sinter process in different solutions. According to their work, the alumina leaching extent up to 100% for CA phase was attained in a mixed NaOH + Na_2CO_3 solution containing 45 g/L Na_2O at 70 °C for 24 h, while $C_{12}A_7$ was optimally leached up to 100% in a solution containing 43–85 g/L Na_2CO_3 at 50–70 °C for 24 h. It is obvious that the leaching duration is depending on the amount of the reacted slags. Bo et al. (2015) showed the synergistic effect of $C_{12}A_7$ and CA mixtures on alumina leaching property, and Sun et al. (2014) investigated the leachability of $C_{12}A_7$ phase in NaOH and Na_2CO_3-containing solution (7 g/L and 120 g/L, respectively) at 75 °C for 30 min where the phase was synthesized at different holding time. In our previous study (Azof et al., 2017), we showed the effect of leaching temperature and duration on the leaching extent of three calcium aluminate phases: CA_2, CA, and C_3A. Also, it is shown that the less leachable calcium aluminate phase may affect the leachability of other phases, with the leachability order from high to the low order being CA, C_3A, and CA_2 phase.

Based on the literature, the $C_{12}A_7$ phase is known as one of the leachable phases in the $CaO\text{-}Al_2O_3$ system. This phase was reported as a metastable phase (Imlach et al., 1971; Nurse et al., 1965a, 1965b). Haccuria et al. (2016) claimed that the metastable $C_{12}A_7$ phase formation is not formed in a $CaO\text{-}Al_2O_3$ system under a dry-inert (99.999%Ar) atmosphere. However, the researchers who investigated the leachability of this phase have not mentioned about its instability (Blake et al., 1966; Bo et al., 2014; Bo et al., 2011; Fursman and Mauser, 1968; Sun et al., 2010; Yu et al., 2012; Zhang et al., 2016; Zhou et al., 2013). It is worth noting that these researchers could attain a stable $C_{12}A_7$ phase from lime-soda sintering or smelting-reduction process.

In the Pedersen leaching process, soluble calcium aluminate phases are imperative for successful alumina extraction with high yield. However, comprehensive information on the leaching behavior of synthetic calcium aluminate slags in caustic solution with different conditions, i.e., concentration, solution, temperature, leaching duration, have not been reported as the process was alive many years ago (1928–1969) and there were confidentiality concerns. Therefore, these have motivated us to study the stability of $C_{12}A_7$ and other calcium aluminate phases produced from $CaO\text{-}Al_2O_3$ slags, and their leaching behavior at specific conditions for alumina recovery.

2. Experimental procedure

The experimental studies were divided into (1) slag composition selection, (2) smelting and slag making, (3) leaching of the slags, and (4) characterization of the leaching products. They are described in details in the following.

2.1. Slag composition selection and preparation

In FactSage™ pure substances (FactPS) database of the $CaO\text{-}Al_2O_3$ system, the available condensed phases at room temperature and 1 atm are CaO, C_3A, CA, CA_2, $CaAl_{12}O_{19}$ (CA_6), and Al_2O_3. Whereas, $C_{12}A_7$ does not exist in the database, which is likely because of its metastable behavior as mentioned previously in section 1. However, as we want to assess the leachability of several calcium-aluminate phases in the $CaO\text{-}Al_2O_3$ system, including $C_{12}A_7$, we should have a phase diagram which includes this phase. By using the FactSage™ FactPS database and an additional thermochemistry data of $C_{12}A_7$ after Hallstedt (1990) we established a phase diagram of the $CaO\text{-}Al_2O_3$ system that includes $C_{12}A_7$ phase as seen in Fig. 2. Moreover, five different compositions of the slags were chosen in the range of 33–60 wt%CaO.

Pure CaO and $\alpha\text{-}Al_2O_3$ powders were used to make a mass of 50 g mixture thoroughly inside a mixing-jar with ceramic balls for each of the targeted slag composition, which is shown in Table 1. These slag compositions were chosen to produce different amounts of various calcium-aluminate phases in each slag, which are also given in Table 1, as calculated using the phase diagram of Fig. 2.

2.2. Slag production

The mixtures of powders were poured into graphite crucibles with about 30 mm and 50 mm of inner diameter and height. These crucibles were then put into a larger graphite crucible as illustrated schematically in Fig. 3, and it was put in an open 75-kVA induction furnace and heated slowly at the rate of 30 °C/min until it reached 1650 °C. The smelting duration was 30 min at this temperature and subsequently the furnace power was turned off, while the crucible was kept in the furnace to solidify and cool down the slags slowly to the room temperature. This was done in exposure to air, the cooling rate from 1650 to 1300 °C was about 34–37 °C/min. The thermocouple used in this study was tungsten/rhenium (C-type) which was encapsulated by alumina and graphite insulation tubes.

The obtained slags were pulverized employing vibratory ring mill Retsch RS-200 at 800 rpm for one minute. Size of the particles was then measured using laser particle analyzer Horiba LA-960 in a wet analysis (isopropanol with refractive index 1.378) based on volume distribution. Before the laser measurement, an ultrasound vibration was run 4 ± 1 min.

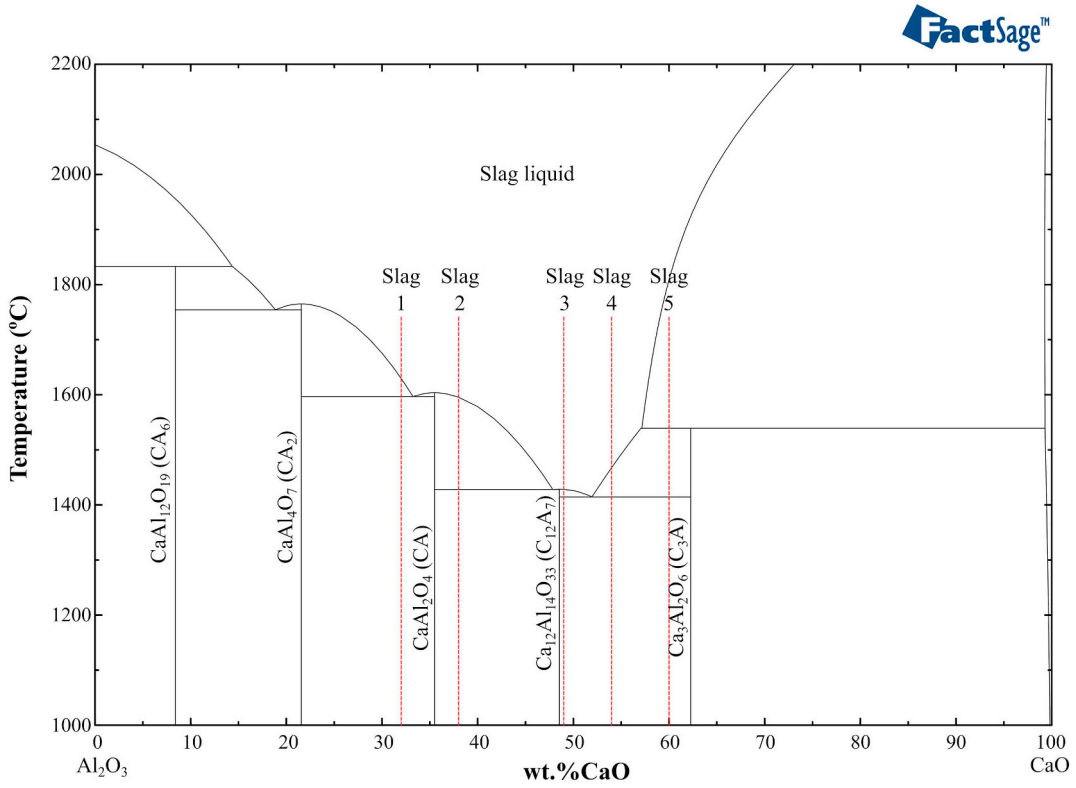

Fig. 2. Phase diagram of the CaO-Al_2O_3 system as constructed in FactSage™ for this study.

Table 1
Compositions of the slags and the estimated co-existing phases.

Sample name	Raw material ratio		Phase in equilibrium (based on phase lever-rule)
	CaO (wt %)	Al_2O_3 (wt %)	
Slag 1	33	67	82.2 wt%CA and 17.8 wt%CA_2
Slag 2	38	62	80.7 wt%CA and 19.3 wt%$C_{12}A_7$
Slag 3	49	51	96.6 wt%$C_{12}A_7$ and 3.4 wt%C_3A
Slag 4	54	46	60.2 wt%$C_{12}A_7$ and 39.8 wt%C_3A
Slag 5	60	40	83.5 wt%C_3A and 16.5 wt%$C_{12}A_7$

2.3. Leaching of the slag

A mass of 1 ± 0.05 g of slag for each of leaching experiments with 20 mL/g of liquid to solid ratio (L/S) was used. Pedersen (1927) stated that the alumina recovery from slags containing calcium aluminate phases could proceed in either sodium carbonate or sodium hydroxide solution as in the Bayer process. In the current study, two different solutions, which are Na_2CO_3 and Na_2CO_3 + NaOH, were used to observe the leaching mechanism and the alumina extraction extent in determined conditions. Our previous study in the leachability of CA and CA_2 phase (Azof et al., 2017) indicated a satisfactory alumina recovery of > 90% for CA phase. Therefore, we used the same parameters for the present study: 120 g/L of Na_2CO_3 and 7 g/L of NaOH for the leaching solutions, 45–75 °C for the leaching temperature, 10–120 min for the leaching duration, and 400 rpm for the stirring magnetic speed. The leaching experiment was performed inside an open beaker glass, which was heated on top of a hot plate as seen schematically in Fig. 4. The loss of solution due to the evaporation was neglected, and in order to minimize the loss, we contained the top of the beaker by using a plastic paraffin film. At the end of leaching, the leachate and the residue were filtered by an ashless grade of quantitative filter paper. The pregnant liquid solution (PLS) was stored in a vial, whereas, the residue was stored in a dryer at 100 °C for an overnight to remove the contained moisture.

2.4. Characterization of the slags and products

High-resolution imaging, Energy Dispersive Spectroscopy (EDS) analysis, and X-ray element mapping of slags and leaching residues were undertaken by using Hitachi SU6600™ Scanning Electron Microscope (SEM). Large slag particles were mounted by epoxy, polished, and carbon coated for SEM study, whereas slags powders were put on a particular carbon substrate for a morphology observation using the same SEM. Phase identification of the slags and residues were done by a Bruker D8 A25 DaVinci™ X-ray Diffraction (XRD) machine with CuKα radiation, between 10 and 75° diffraction angle, 0.01° step size, and 2.5° for both primary and secondary soller slit. The identification and quantitative phase analysis of the obtained XRD peaks were done by using DIFFRAC.EVA v.3 and TOPAS v.5 software based on the Rietveld method, respectively. Chipera and Bish (2013) claimed that the method is suitable for a quantitative phase analysis (QPA) as this method relies on the assumption that all phases in the sample are crystalline, which is relevant in the current study as later seen in the XRD results, where the slags do not contain amorphous phase. Literature (Guirado et al., 2000) showed that a QPA performed by Rietveld method in aluminous cement was somewhat in agreement with those performed by X-ray Fluorescence (XRF). Also, Inductively Coupled Plasma-High Resolution-Mass Spectrometer (ICP-HR-MS) Agilent 8800™ was used to analyze the compositions of the PLS.

3. Theoretical evaluation

In order to obtain a proper understanding of the leaching property of the slags and the effect of the reactions to the pH changes, we need to elaborate the leaching thermochemistry, and both pH and aluminum extraction yield calculations.

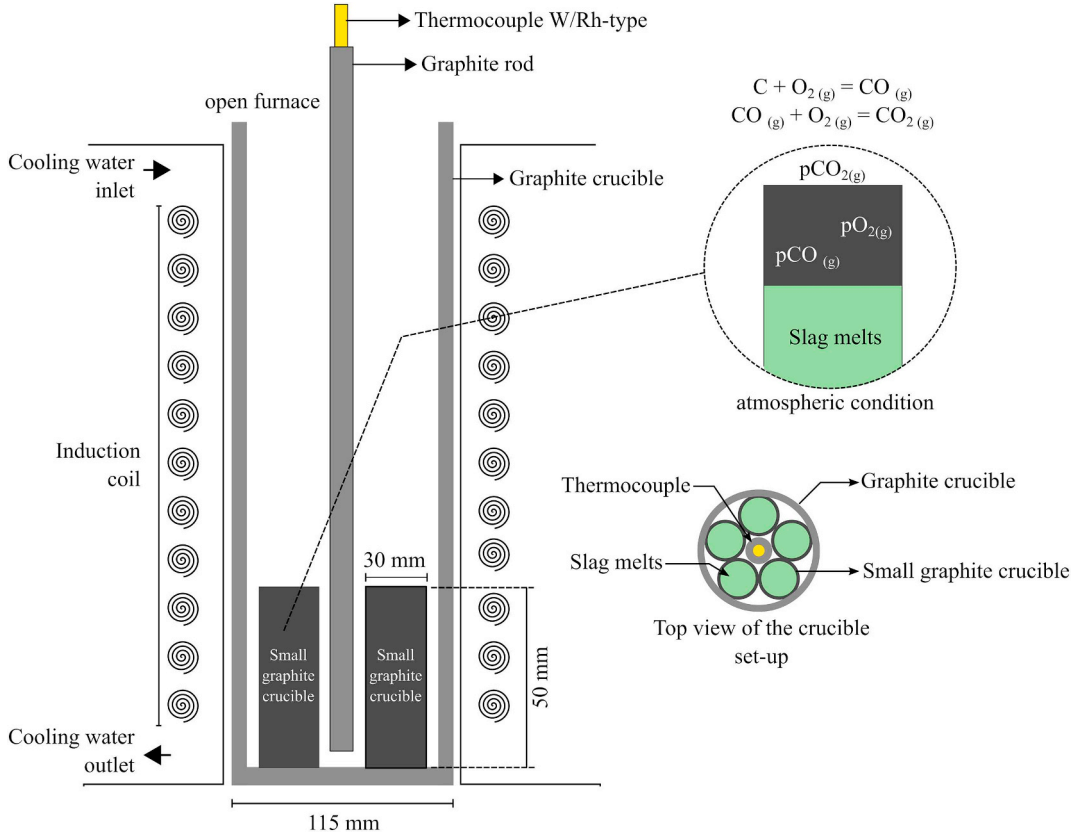

Fig. 3. A schematic of the slag making setup in induction furnace.

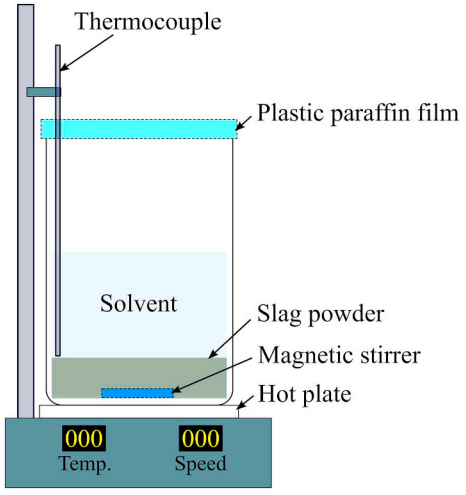

Fig. 4. A schematic of the leaching setup.

3.1. Leaching reactions

The leaching reactions between CA, CA_2, C_3A, and $C_{12}A_7$ phases and sodium carbonate solution can be written as shown in reactions (1)–(4), respectively (Azof et al., 2017; Blake et al., 1966). The Gibbs energy of reactions at 25 °C is calculated by using HSC Chemistry™, a thermodynamic software.

$$CaAl_2O_{4\,(s)} + Na_2CO_{3\,(aq)} = 2NaAlO_{2\,(aq)} + CaCO_{3\,(s)} \quad (1)$$

$$\Delta G^{\circ}{}_{25°C} = -58.2\ \text{kJ/mol}\ CaAl_2O_4.$$

$$CaAl_4O_{7\,(s)} + Na_2CO_{3\,(aq)} + 2NaOH_{(aq)} + 7H_2O_{(l)} = 4NaAl(OH)_{4\,(aq)} + CaCO_{3\,(s)} \quad (2)$$

$$\Delta G^{\circ}{}_{25°C} = -51.0\ \text{kJ/mol}\ CaAl_4O_7$$

$$Ca_3Al_2O_{6\,(s)} + 3Na_2CO_{3\,(aq)} + 2H_2O_{(l)} = 2NaAlO_{2\,(aq)} + 3CaCO_{3\,(s)} + 4NaOH_{(aq)} \quad (3)$$

$$\Delta G^{\circ}{}_{25°C} = -199.1\ \text{kJ/mol}\ Ca_3Al_2O_6$$

$$Ca_{12}Al_{14}O_{33\,(s)} + 12Na_2CO_{3\,(aq)} + 5H_2O_{(l)} = 14NaAlO_{2\,(aq)} + 12CaCO_{3\,(s)} + 10NaOH_{(aq)} \quad (4)$$

$$\Delta G^{\circ}{}_{25°C} = -745.2\ \text{kJ/mol}\ Ca_{12}Al_{14}O_{33}$$

As seen above, CA, C_3A, and $C_{12}A_7$ phase can be leached in a solution containing Na_2CO_3. The product of the reactions contains:

(1) Sodium aluminate in hydrated ($NaAl(OH)_4$) or un-hydrated ($NaAlO_2$) aqueous phase,
(2) $NaOH_{(aq)}$ such as in reactions (3) and (4), and.
(3) $CaCO_3$-containing residue (simply named as residue)

In reaction (2), to leach one mole of the CA_2 phase, we need one mole of $Na_2CO_{3\,(aq)}$ and two moles of $NaOH_{(aq)}$, while other calcium aluminates need no addition of $NaOH_{(aq)}$ in their leaching reactions. In Fig. 5, we can see the equilibrium amount of thermodynamic reaction (2) at temperature 25–100 °C in 1 atm as calculated using HSC Chemistry™ in Equilibrium Compositions module. The modeling is based on the Pitzer (1973) theory on calculating the activity coefficient of electrolytes. The input amount and output species that correspond to Fig. 5 is shown in Table 2. The input species and the amount used in the calculation are chosen as an attempt to indicate the experimental

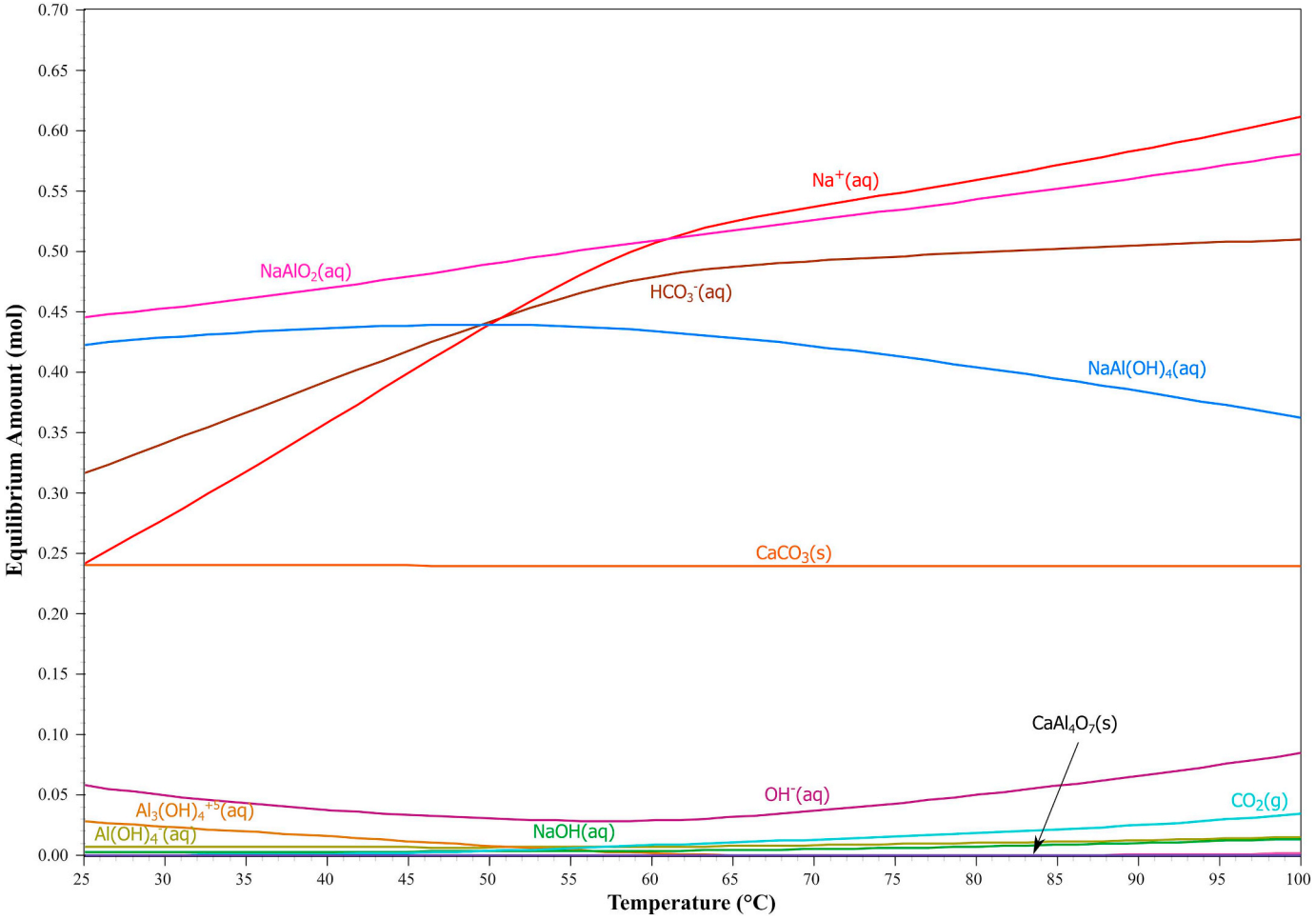

Fig. 5. The equilibrium amount of the leaching reaction of CA_2 phase at a temperature range of 25–100 °C.

Table 2
Input amount and output species that are used in the equilibrium calculation.

Input species	Phase	Mass (g)	Mass (mol)
H_2O	Liquid	1000	55.51
$CaAl_4O_7$	Solid	50	0.24
Na_2CO_3	Aqueous	120	1.13
OH^-	Aqueous	1.7×10^{-2}	1×10^{-3}
H^+	Aqueous	1×10^{-3}	1×10^{-3}
O_2	Gas	3.2×10^{-4}	1×10^{-5}
Output species			
$Al(OH)_{2(aq)}^{+}$	$Ca(OH)_{2(s)}$	$CH_2O_{2(g)}^{+}$	$NaOH_{(aq)}$
$Al(OH)_{3(aq)}$	$Ca_{(aq)}^{+2}$	$CH_2OH_{(g)}^{+}$	$NaAl(OH)_{4\ (aq)}$
$Al(OH)_{4(aq)}^{-}$	$Ca_3Al_2O_{6(s)}$	$CH_2OO_{(g)}^{-}$	$O_{2(aq)}$
$Al_{13}O_4(OH)_{24(aq)}^{+7}$	$CaAl_{12}O_{19(s)}$	$CH_3COO_{(aq)}^{-}$	$O_{2(g)}$
$Al_2(OH)_{2(aq)}^{+4}$	$CaAl_2O_{4(aq)}$	$CH_3O_{(g)}^{-}$	$O_{2(g)}^{-}$
$Al_2O_{(g)}^{+}$	$CaAl_2O_{4(s)}$	$CH_3O_{2(g)}^{-}$	$OH_{(aq)}$
$Al_2O_{2(g)}^{+}$	$CaAl_4O_{7(s)}$	$CH_3O_{2(g)}^{+}$	$OH_{(aq)}^{-}$
$Al_3(OH)_{4(aq)}^{+5}$	$CaC_2H_3O_{2(aq)}^{+}$	$CH_3OH_{(g)}^{-}$	$OH_{(g)}^{-}$
$AlO_{(g)}^{-}$	$CaC_2H_3O_{3(aq)}^{+}$	$CHO_{(g)}^{+}$	$OH_{(g)}^{+}$
$AlO_{(aq)}^{+}$	$CaCHO_{2(aq)}^{+}$	$CO_{(aq)}$	$H_2O_{(l)}$
$AlO_{(g)}^{+}$	$CaCO_{3(aq)}$	$CO_{(g)}$	$12CaO{\cdot}7Al_2O_{3(s)}$
$AlO_{2(g)}^{-}$	$CaCO_{3(s)}$	$CO_{2(aq)}$	$2CaO{\cdot}Al_2O_{3(s)}$
$AlOH_{(g)}$	$CaHCO_{3(aq)}^{+}$	$CO_{2(g)}$	$3CaO{\cdot}Al_2O_{3(s)}$
$AlOH_{(g)}^{+}$	$CaO{\cdot}2Al_2O_{3(s)}$	$H_{(aq)}^{+}$	$3CaO{\cdot}Al_2O_3{\cdot}10.2H_2O_{(s)}$
$AlOH_{(aq)}^{+2}$	$CaO{\cdot}Al_2O_{3(s)}$	$HC_2O4_{(aq)}^{-}$	$3CaO{\cdot}Al_2O_3{\cdot}11.6H_2O_{(s)}$
$C_2H_3O_{(g)}^{+}$	$CaOH_{(aq)}^{+}$	$HCO_{2(aq)}^{-}$	$3CaO{\cdot}Al_2O_3{\cdot}6H_2O_{(s)}$
$C_2H_3O_{3(aq)}^{-}$	$CaOH_{(g)}^{+}$	$HCO_{3(aq)}^{-}$	$3CaO{\cdot}Al_2O_3{\cdot}8H_2O_{(s)}$
$Ca(CHO_2)_{2(aq)}$	$CH_2O_{(g)}^{-}$	$Na_{(aq)}^{+}$	$3CaO{\cdot}Al_2O_3{\cdot}CaCO_3{\cdot}10.68H_2O_{(s)}$
$Ca(OH)_{2(aq)}$	$CH_2O_{2(g)}^{-}$	$NaAlO_{2(aq)}$	$4CaO{\cdot}Al_2O_3{\cdot}13H_2O_{(s)}$

leaching conditions, i.e., L/S = 20, 120 g/L Na_2CO_3, etc. The same amount of $H^+_{(aq)}$ and $OH^-_{(aq)}$ is introduced to maintain the electronic neutrality of the system. Also, a minor addition of $O_{2\ (g)}$ is necessary to help the Gibbs solver find the equilibrium composition.

In equilibrium, Fig. 5 indicates that the amount of CA_2 is considerably low compared to the sodium aluminate-containing aqueous phase at temperature 25–100 °C. This means that according to their thermodynamic properties the sodium aluminate-containing aqueous phase is more stable in the system than the slag. However, later we will see that the leaching property results based on the experiment show that side reactions could happen during the leaching and some calcium aluminate phases could be identified as the less leachable ones.

3.2. The pH calculation

The leaching agent was prepared by dissolving 120 g of Na_2CO_3 in 1 L of water (1.1 M Na_2CO_3). Therefore, the complete dissolution of Na_2CO_3 is shown by reaction (5).

$$Na_2CO_{3\,(aq)} = 2Na^+_{(aq)} + CO_3{}^{2-}{}_{(aq)} \quad (5)$$

The reaction of sodium cations and water yield a neutral solution. However, the carbonate anions act as weak alkali and can contribute to the pH of the solution as in reaction (6).

$$CO_3{}^{2-}{}_{(aq)} + H_2O_{(l)} = HCO_3{}^-{}_{(aq)} + OH^-{}_{(aq)} \quad (6)$$

As the initial concentration of $CO_3{}^{2-}$ is known, we may set an initial, change, and equilibrium table for the above reaction as Table 3.

Table 3
Initial, change, and equilibrium condition of CO_3^{2-} reaction with water.

Condition	$[CO_3^{2-}]$	$[HCO_3^-]$	$[OH^-]$
Initial	1.1	0	0
Change	-x	+x	+x
Equilibrium	1.1 - x	x	x

Based on the HSC Chemistry™ database, the equilibrium constant (K_b) of reaction (6) is $2.049{\cdot}10^{-4}$, which gives Eq. (7).

$$Kb = \frac{a_{HCO_3^-} \bullet a_{OH^-}}{a_{CO_3^{2-}} \bullet a_{H_2O}} = 2.049{\cdot}10 - 4 \tag{7}$$

Where a_{HCO3-}, a_{OH-}, a_{CO32-}, a_{H2O} are the activities of HCO_3^-, OH^-, CO_3^{2-}, and H_2O in a solution, respectively. Assume the solution is an ideal mixture, then the activity is as same as the molar concentration. Consider the activity of water is unity and, thus, taking into account the equilibrium condition in Table 3, the Eq. (7) becomes Eq. (8).

$$2.049{\cdot}10 - 4 = \frac{x^2}{1.1 - x} \tag{8}$$

The x value is considerably small, thus neglecting x value in denominator gives $x = 0.015$. As $pOH = -\log [OH^-]$ and $pH = 14 - pOH$, then the theoretical pH in the leaching solution is 12.2.

Moreover, if we consider the slags leaching reactions (1)–(4) in the solution, the leaching product (i.e., $NaAlO_2$) can be hydrated with water and produce aluminate ion, whereas in a high pH solution it is in the form of $Al(OH)_4^-$ (Moolenaar et al., 1970), as seen in reaction (9). Furthermore, reaction (3) and (4) give NaOH as the leaching product, which is a strong alkali and can dissociate entirely in the solution as seen in reaction (10).

$$2NaAlO_{2\,(aq)} + 4H_2O_{(l)} = 2Na^+_{(aq)} + 2Al(OH)_4{}^-_{(aq)} \tag{9}$$

$$NaOH_{(aq)} = Na^+_{(aq)} + OH^-_{(aq)} \tag{10}$$

The $NaAlO_2$ aqueous solution could be considered as a weak alkali where the only fraction of it accepts protons from water, which means along with the dissociation of NaOH in reaction (10), both of these reactions most likely increase the pH extent of the leachate during the leaching.

3.3. Aluminum extraction yield

If we have a maximum aluminum leaching extent of each calcium aluminate phase and no materials loss during the experiment due to the evaporation and/or filtration, then based on the slags composition provided in Table 1, we may calculate the maximum extraction of aluminum in the leachate after the leaching treatment as shown in Table 4.

4. Results and discussion

The results obtained about the characteristics of the produced slags, their leaching behavior, and leaching products analysis are presented. Mechanisms related to the leaching of calcium aluminate phases will be discussed, supported by structural modeling of the phases.

Table 4
Maximum extraction of aluminum in the leachate.

Sample	Pulp concentration (g/L)	Aluminum in leachate (g/L)
Slag 1	50	17.7
Slag 2	50	16.4
Slag 3	50	13.5
Slag 4	50	12.2
Slag 5	50	10.6

4.1. Characteristics of the slags

The particle size distribution of each synthesized slag listed in Table 1 is shown in Fig. 6. Consecutively, the mean diameter of Slags 1, 2, 3, 4 and 5 is 7.8 ± 3.9, 7.1 ± 4.5, 26.6 ± 22.8, 5.4 ± 2.2, and 5.3 ± 2.3 μm. Slag 3 has the largest mean diameter of the particle as well as the standard deviation compared to the others as it has an agglomeration-type of particle and not easily disintegrated even though the ultrasound was applied for several minutes. We believe the agglomeration-tendency is caused by the high reactivity of $C_{12}A_7$ phase to the moisture as supported by literature:

(1) Jeevaratnam et al. (1964) and Nurse et al. (1965b) claimed the phase might contain up to 1.3 to 1.4 wt% H_2O at 1100 °C in an air of normal humidity,
(2) Roy and Roy (1960) claimed the $C_{12}A_7$ phase has zeolitic behavior, which means that the phase can absorb and desorb water as a function of temperature (with pH_2O fixed) without structural change,
(3) Thermogravimetric analysis by Hayashi et al. (2002) revealed that in a dry-oxygen environment the $C_{12}A_7$ phase losses its weight for about 1% when heated to 700 °C, and the loss was restored when cooled down to below 700 °C.

The XRD patterns of the obtained slags and the determined phases are presented in Fig. 7. Slag 1 has CA and CA_2 phases, Slag 2 has CA and C_3A phases, Slag 3 has a single $C_{12}A_7$ phase, Slag 4 has C_3A and $C_{12}A_7$ phases, and Slag 5 has C_3A and $Ca_5Al_6O_{14}$ (C_5A_3) phases. Most of the phases are well identified and formed in crystalline form, showing the applied cooling rates were proper for crystallization of the phases. A result of the relative fraction of the obtained phases is also shown in Fig. 7.

Based on the results in Fig. 7, three points are very important to note. First, the similarity of the Slags 1 and 3 compositions to the equilibrium ones as we have calculated based on lever-rule in Table 1. Second, the absence of $C_{12}A_7$ phase in Slags 2 and 5, which is discussed later. Third, the co-existence of C_5A_3 in Slag 5 that was "unrecognizable" in the phase diagram of CaO-Al_2O_3 in Fig. 2, however, it appears in the XRD spectrum.

As of today, $C_{12}A_7$ and C_5A_3 phases are not readily established in the CaO-Al_2O_3 system especially in certain atmospheric conditions as some literature omitted one or both phases in their assessment (Haccuria et al., 2016; Hallstedt, 1990; Jerebtsov and Mikhailov, 2001; Lutsyk et al., 2012; Mao et al., 2006). In our previous study (Azof et al., 2017), we also could not observe the presence of $C_{12}A_7$ phase in a slag produced from the same composition and condition, as we did observe again in this study for Slag 2. Knowing that CA is the dominant phase in Slag 2 (about 80 wt% based on phase lever-rule), and $C_{12}A_7$ is a metastable phase, then dissociation of the unstable $C_{12}A_7$ to C_3A and CA phase at low temperature proposed by Nurse et al. (1965a, 1965b), as shown in reaction (11) might be the reason.

$$2[Ca_{12}Al_{14}O_{33\,(s)}] = 5[Ca_3Al_2O_{6\,(s)}] + 9[CaAl_2O_{4\,(s)}] \tag{11}$$

The stable form of $C_{12}A_7$ phase in Slags 3 and 4 may be due to a relatively similar CaO: Al_2O_3 molar ratio of these slags to $C_{12}A_7$ phase. Also, the presence of "guest" anions, such as OH^- (Roy and Roy, 1960), halide ions, i.e., Cl^-, F^- (Jeevaratnam et al., 1964), and S^{2-} (Zhmoidin and Chatterjee, 1984), could favorably stabilize the phase. The latter suggestion needs further investigation to obtain more evidence on the stabilizing element that presents in the slags.

Concerning the C_5A_3 phase co-existence in Slag 5, Shepherd et al. (1909) were first among the researchers who reported the presence of the phase in the CaO-Al_2O_3 system. Subsequently, Rankin and Wright (1915) observed C_5A_3 phase with a composition of 47.8 wt%CaO and 52.2 wt%Al_2O_3 and said that it could form in either stable or unstable monotropic form. The stable form melts congruently at 1455 ± 5 °C,

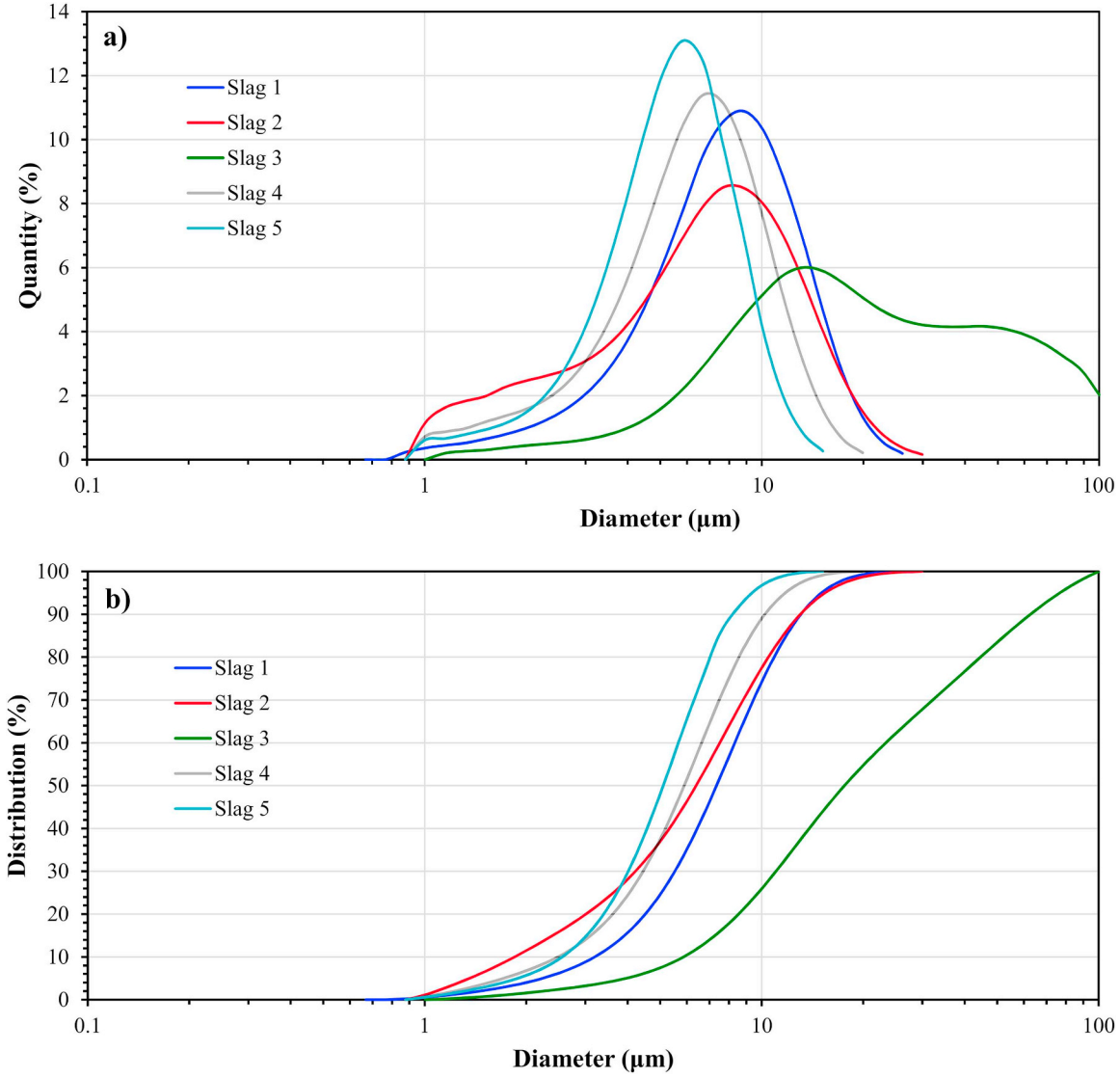

Fig. 6. Laser particle size measurement based on (a) differential and (b) accumulative type of the obtained slags.

and it could form a eutectic mixture with C_3A ($CaO:Al_2O_3$ mass ratio = 50:50) at 1395 ± 5 °C. This structure gave rise of some discussions and debate among scientists, Büssem (1936) said that the measured density of C_5A_3 phase does not agree with its chemical formula, and they proposed $C_{12}A_7$ formula instead of it. Thorvaldson and Schneider (1941) investigated the composition of the aluminate obtained by thermal decomposition of $3CaO{\cdot}Al_2O_3{\cdot}6H_2O$ ($Ca_3Al_2(OH)_{12}$) and showed that the free lime amount produced from $Ca_3Al_2(OH)_{12}$ dehydration suits with the composition of $C_{12}A_7$ than C_5A_3, correspondingly. In contrary, Aruja (1957) measured the density of two single-crystals of C_5A_3 and said that the orthorhombic C_5A_3 formula gives a better fit than $C_{12}A_7$, and the XRD pattern of both C_5A_3 and $C_{12}A_7$ showed that the compounds show no resemblance. Zhmoidin and Chatterjee (1984) stated that it is possible under conditions of deficit oxygen $C_{12}A_7$ is unstable, and C_5A_3 phase stabilizes with denser (3.03 g/cm^3) orthorhombic structure. Later on, Brisi et al. (1986) confirmed the possibility of making C_5A_3 from the $C_{12}A_7$ phase in solid-state reaction provided that low oxygen partial pressure and water vapor be preserved. In this study, the presence of reducing gas ($CO_{(g)}$) during smelting trials due to the use of graphite crucible could reduce the oxygen partial pressure and is believed to stimulate the stability of C_5A_3 in Slag 5.

4.2. Leaching behavior of the slags

The obtained leaching residue was analyzed to characterize the leaching behavior of the existing phases in the slags and the effect of dissolved slags on the pH of the leachate.

4.2.1. Phases of the leached residue

Fig. 8 shows the XRD patterns of each residue obtained after filtering the leachates. As expected, residue from each slag contains a considerably high amount of $CaCO_3$, which is in the form of calcite and vaterite, and some remaining undissolved phases. Also, $Al(OH)_3$ in bayerite form and $Ca_3Al_2(OH)_{12}$ phase are observed in some of the residues. The formation of solid $Al(OH)_3$ in this stage could be detrimental as it decreases the alumina yield in the leachate. While the latter phase is usually prepared in the Bayer process, which could assist the removal of impurities from the pregnant liquor (Whittington and Cardile, 1996). In this study, we may say that both $Al(OH)_3$ and $Ca_3Al_2(OH)_{12}$ can be formed due to the hydration of CA in water during the leaching treatment, which was proposed earlier by Lundquist and Leitch (1963a) as in reaction (12).

$$3[CaAl_2O_{4\,(s)}] + 12H_2O_{(l)} = Ca_3Al_2(OH)_{12\,(s)} + 4Al(OH)_{3\,(s)} \quad (12)$$

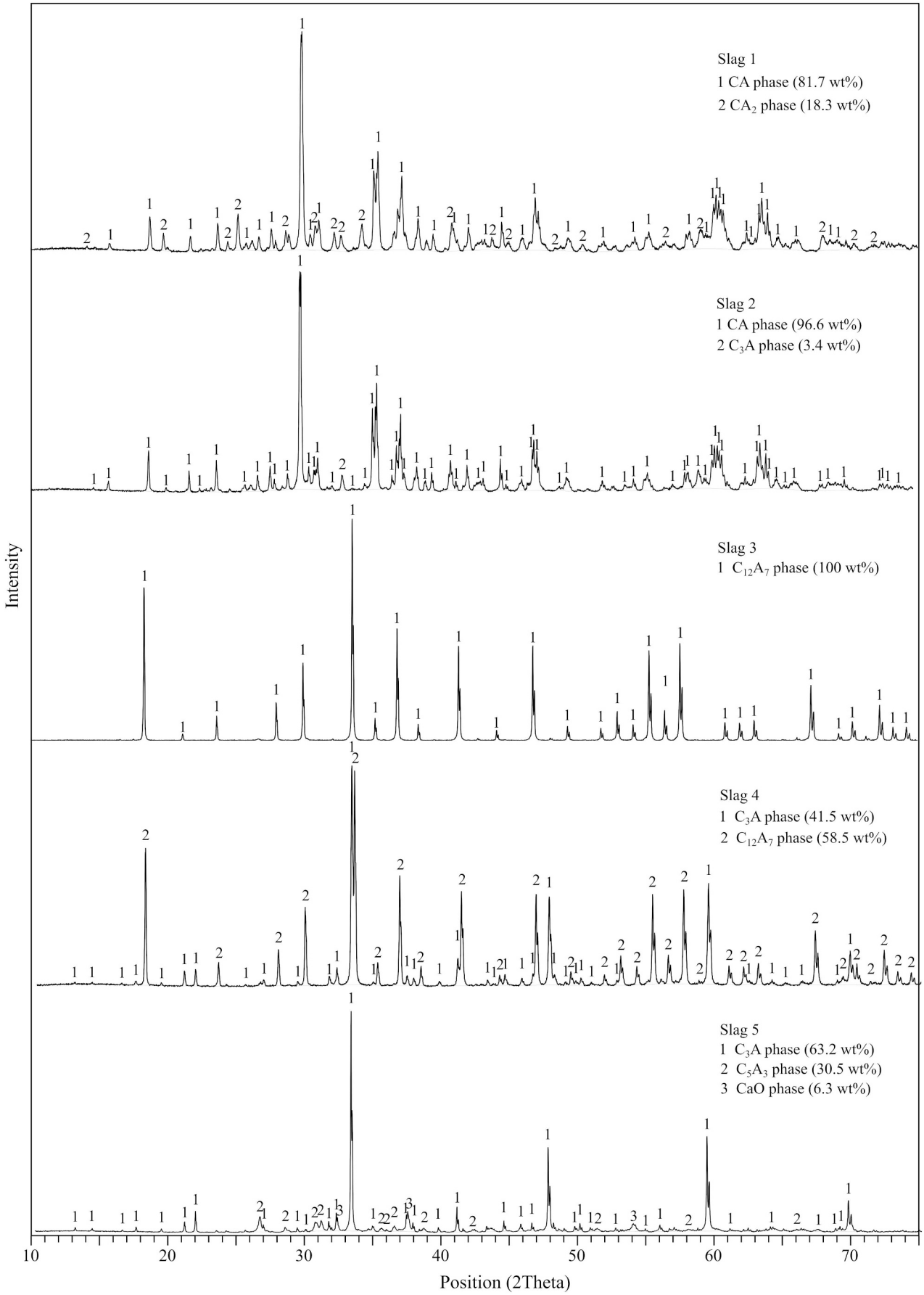

Fig. 7. XRD pattern of the obtained slags with the quantified compositions of the phases.

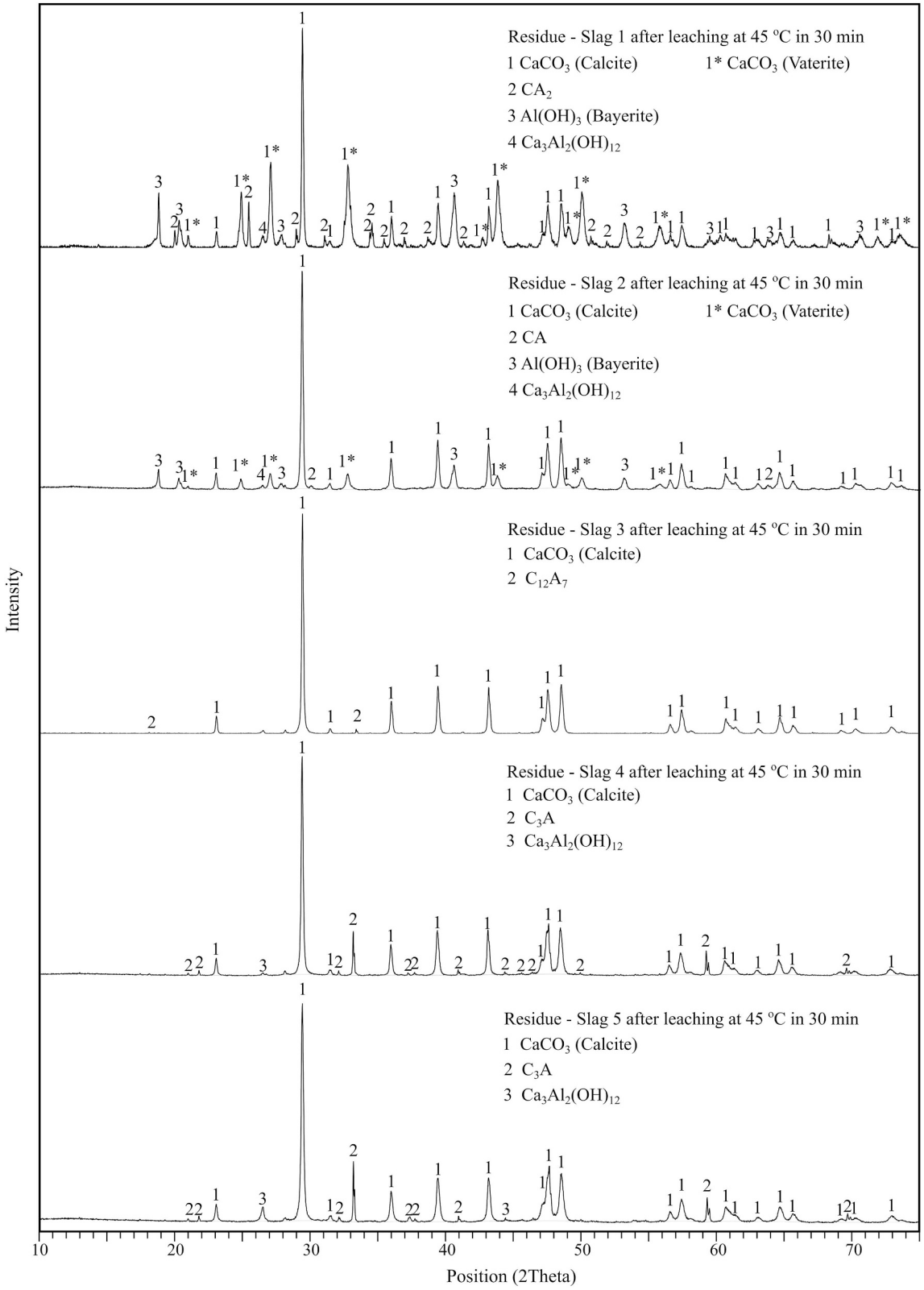

Fig. 8. XRD results of the residue of the slags after the leaching treatment at 45 °C in 30 min.

$\Delta G^{\circ}_{25°C} = -27.0$ kJ/mol $CaAl_2O_4$

The formation of $Ca_3Al_2(OH)_{12}$ in the residue of Slag 5 is not necessarily producing $Al(OH)_3$ as in the case of Slags 1 and 2. We suggest that the hydration of the C_3A phase in Slag 5 may produce $Ca_3Al_2(OH)_{12}$ as seen in reaction (13), which could explain the absence of $Al(OH)_3$ in the residue. Furthermore, the presence of free-CaO in Slag 5 could enhance the amount of $Ca_3Al_2(OH)_{12}$ after the leaching, as was proposed by Whittington et al. (1997) who claimed that the addition of CaO in sodium aluminate solution produces $Ca_3Al_2(OH)_{12}$ as we see in reaction (14).

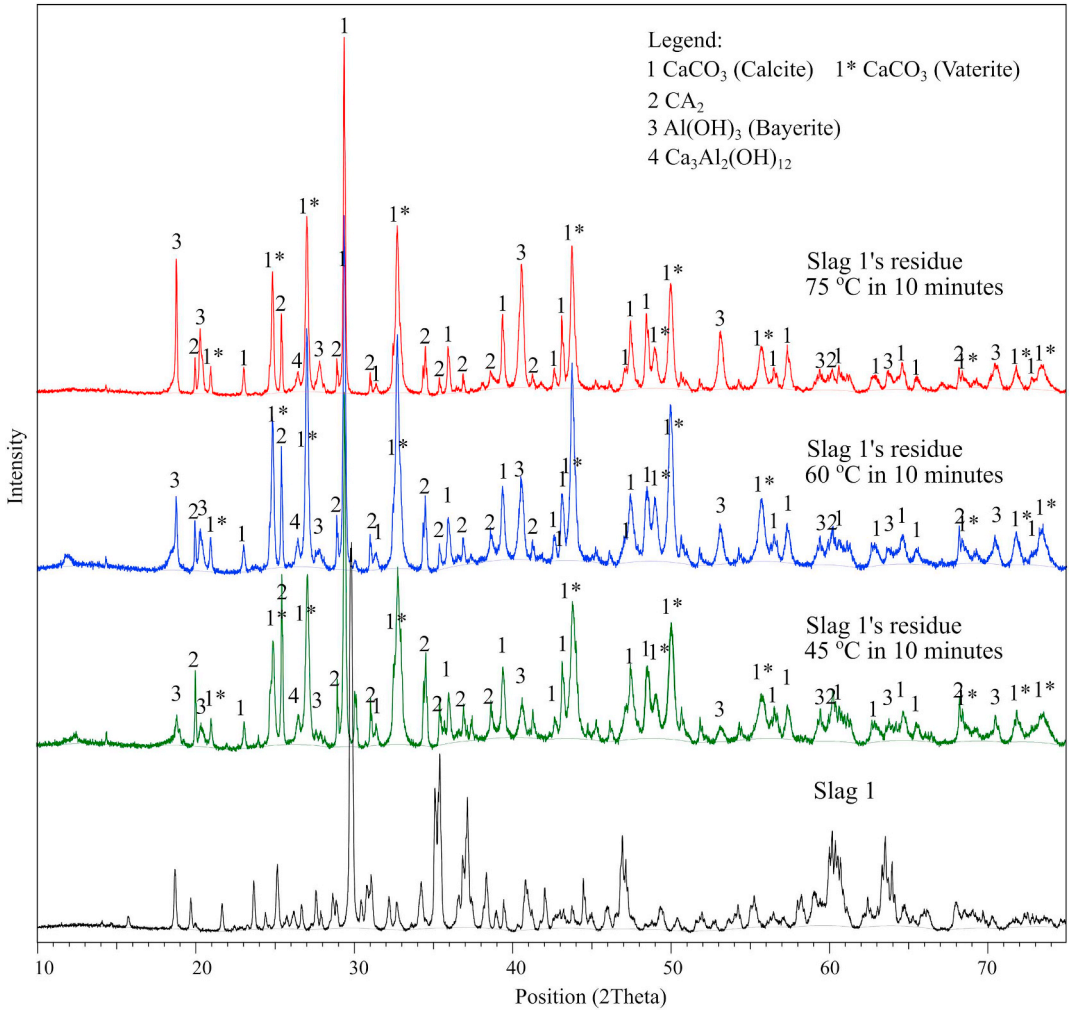

Fig. 9. XRD patterns of the residue obtained from Slag 1 after the leaching treatment in Na_2CO_3 solution at 45, 60, and 75 °C in 10 min.

$$Ca_3Al_2O_{6\,(s)} + 6H_2O_{(l)} = Ca_3Al_2(OH)_{12\,(s)} \quad (13)$$

$$\Delta G^{\circ}{}_{25°C} = -134.3 \text{ kJ/mol } Ca_3Al_2O_6$$

$$2NaAl(OH)_{4\,(aq)} + 3CaO_{(s)} + 3H_2O_{(l)} = Ca_3Al_2(OH)_{12\,(s)} + 2NaOH_{(aq)} \quad (14)$$

$$\Delta G^{\circ}{}_{25°C} = -49.9 \text{ kJ/mol CaO.}$$

4.2.2. Effect of temperature

Fig. 9 shows the XRD patterns of Slag 1 residue after being leached by Na_2CO_3 solution for 10 min at 45, 60, and 75 °C. The most distinct peaks observed from the three different temperatures are $Al(OH)_3$ and CA_2 peaks. It seems that by increasing temperature the intensities of $Al(OH)_3$ peaks become more apparent. Lundquist and Leitch (1963b) stated that the temperature gives modest effect to the precipitation of $Al(OH)_3$ when CA is leached in water. However, in principle, the formation of $Al(OH)_3$ in the Na_2CO_3 solution is as same as in the water, where it employs the hydration of CA (reaction (12)). We suggest that the undesirable precipitation may be accelerated by thermal energy.

On the other hand, by increasing the temperature, the CA_2 phase becomes more leachable as the intensity of its peaks decreases. This is supported by our former observation (Azof et al., 2017) that stated the leaching extent of CA_2 phase is markedly increased after about 60 °C. Therefore, it can be concluded here that the effect of leaching temperature on the alumina extraction extent is likely dependent on both the calcium aluminates composition and the solvent characteristics.

4.2.3. Effect of sodium hydroxide addition

In the original method of Pedersen (1927), "free sodium hydroxide" is used to prevent the dissolution of silica in pregnant solution, which is not of the interest in the current CaO-Al_2O_3 system. However, Pedersen claimed that if a larger proportion of "free sodium hydroxide" is used, the rate of alumina dissolution and the ratio of alumina to soda in the solution are decreased. As Pedersen did not mention specifically the amount of "free sodium hydroxide," we introduced NaOH in Na_2CO_3 solution about two times than the stoichiometry required in Slag 1 and 2 in our previous study (Azof et al., 2017), to validate Pedersen's statement.

Figs. 10 and 11 show the comparison of XRD patterns of the residues produced from Slags 1 and 2 in different solutions. As shown, the peaks intensity of $Al(OH)_3$ and $Ca_3Al_2(OH)_{12}$ in the two residues are noticeably low. The dissolution process of these phases in NaOH-containing solution is shown in reaction (15) and (16). The first one is a typical reaction in the pressure leaching of the Bayer process (Bayer, 1894; Safarian and Kolbeinsen, 2016a). While the latter is proposed by Alekseev (1982) that in NaOH solution (6–200 g/L) and at a certain temperature (25–90 °C) the $Ca_3Al_2(OH)_{12}$ may be unstable and dissociates to $Ca(OH)_2$ and NaAl(OH).

$$Al(OH)_{3\,(s)} + NaOH_{(aq)} = NaAl(OH)_{4\,(l)} \quad (15)$$

$$\Delta G^{\circ}{}_{25°C} = -7.0 \text{ kJ/mol } Al(OH)_3$$

$$Ca_3Al_2(OH)_{12\,(s)} + 2NaOH_{(aq)} = 2NaAl(OH)_{4\,(aq)} + 3Ca(OH)_{2\,(s)} \quad (16)$$

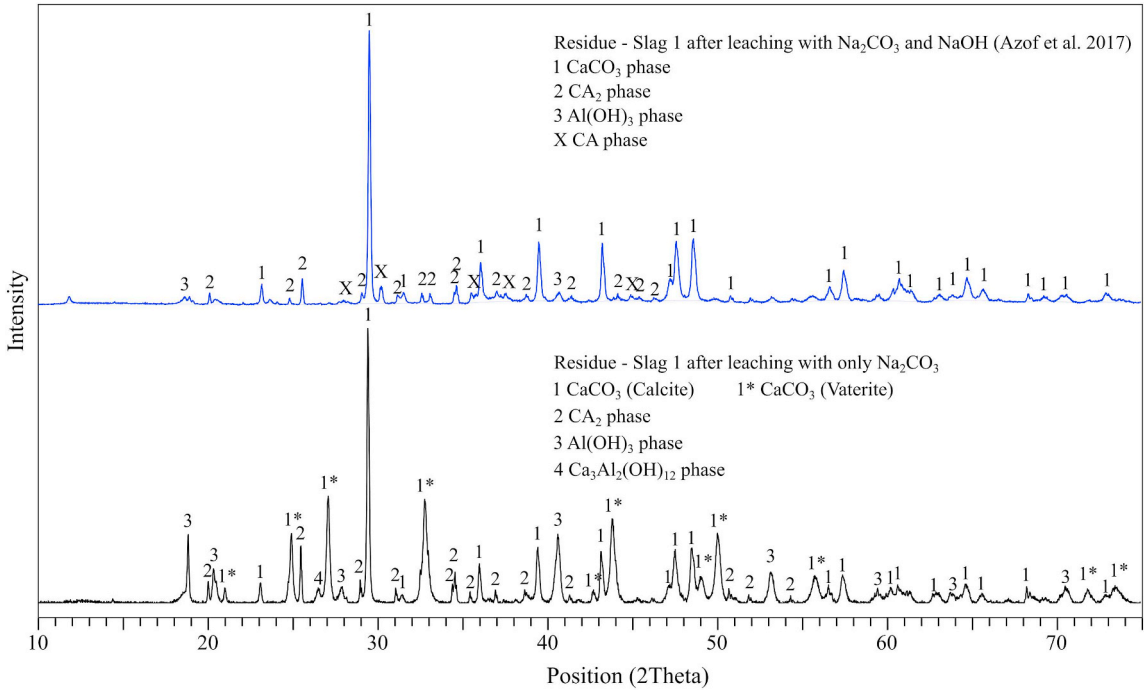

Fig. 10. XRD pattern of the obtained residues from Slag 1 after leaching in different solvents with the same temperature and duration.

$\Delta G^{\circ}_{25°C} = -22.9$ kJ/mol $Ca_3Al_2(OH)_{12}$

In reaction (12), we see that the CA phase can be hydrated in water and form $Ca_3Al_2(OH)_{12}$. However, it should be considered here that in a solution with some extent of NaOH concentration, the CA phase may also react with NaOH to form $Ca_3Al_2(OH)_{12}$ that leads to the alumina losses. Nevertheless, it gives sufficient OH^- ions to prevent $Al(OH)_3$ from precipitating (R.V. Lundquist and Leitch, 1963), as shown in reaction (17).

$$3[CaAl_2O_4]_{(s)} + 4NaOH_{(aq)} + 12H_2O_{(l)} = Ca_3Al_2(OH)_{12\,(s)} + 4NaAl(OH)_{4\,(aq)} \quad (17)$$

$\Delta G^{\circ}_{25°C} = -36.42$ kJ/mol $CaAl_2O_4$.

This means if we take into account the reaction of calcium aluminate in sodium carbonate and sodium hydroxide as in reactions (1) and (17), respectively, we can predict the equilibrium of the precipitated $CaCO_3$ and $Ca_3Al_2(OH)_{12}$ in residue based on the amount of NaOH and

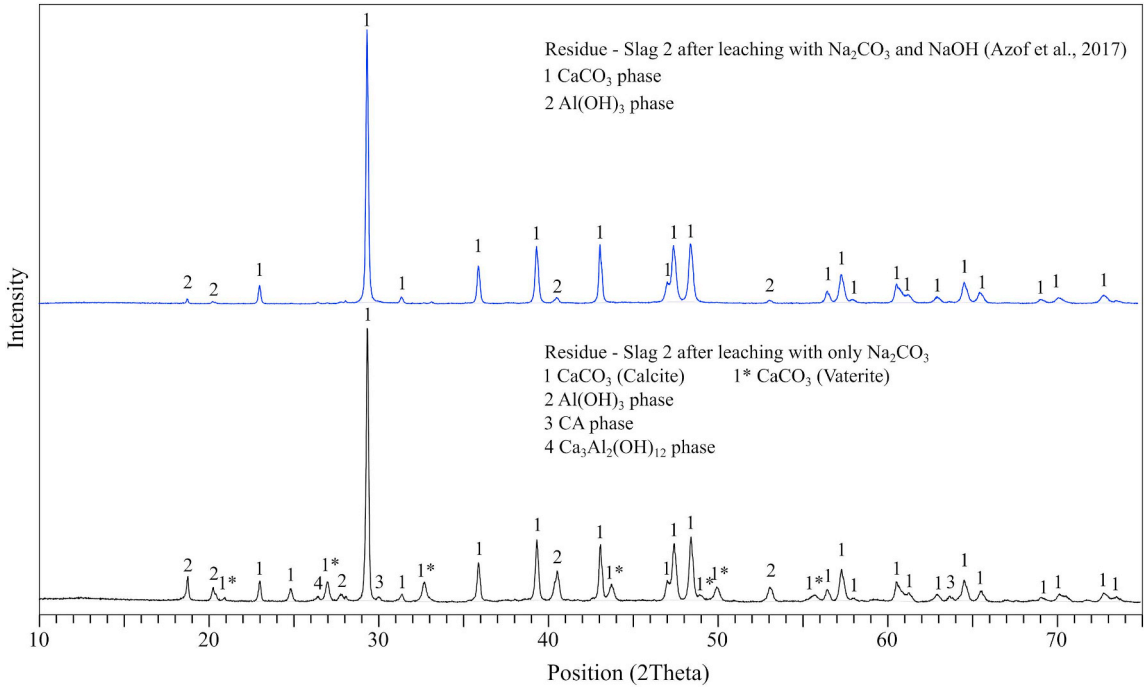

Fig. 11. XRD pattern of the obtained residues from Slag 2 after leaching in different solvents with the same temperature and duration.

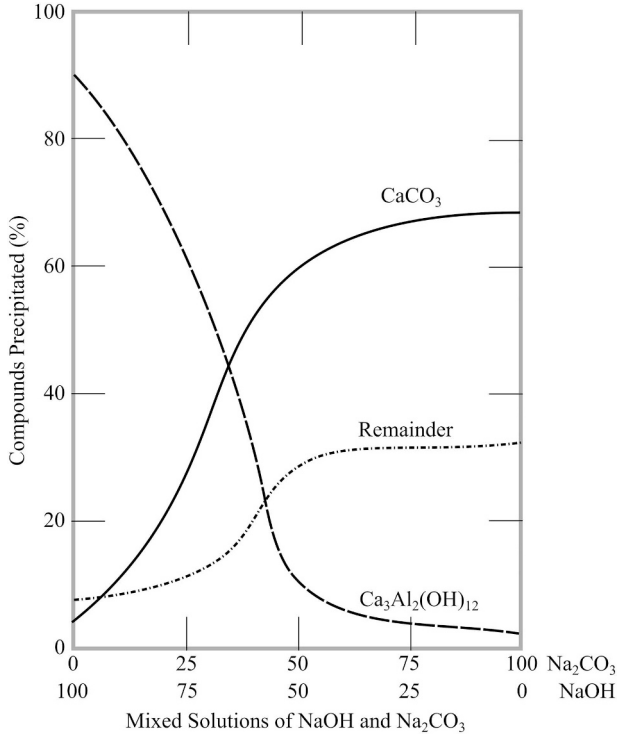

Fig. 12. Mixed solutions of NaOH and Na_2CO_3 in accordance with the precipitated compounds as reconstructed from Lundquist and Leitch (1963).

Na_2CO_3 in the mixed solution. Fig. 12 shows the relationship between the mixed solution ratio of NaOH:Na_2CO_3 to the number of precipitated compounds in the residue as reconstructed from Lundquist and Leitch (1963). The figure indicates that the carbonate anions in the solution are necessitated to the alumina loss prevention as it reacts with the calcium cations and replacing the hydroxyl ion, $Al_2(OH)_{12}{}^{2-}$, so that $CaCO_3$ precipitation is more favorable than the $Ca_3Al_2(OH)_{12}$ precipitation.

4.2.4. The solution pH and aluminum recovery

We measured the pH changes in the solution before and after the leaching of Slags 1–5 at certain temperatures. The pH meter was calibrated with buffer pH 4.0 and 7.0 before use. The pH was measured for the blank solution that consisted of 120 g/L Na_2CO_3 at 25 °C is 11.4 ± 0.1. Moreover, the pH range of the leachate is 12.5–12.9, which changes according to the leaching temperature and OH^- concentration. The aluminum amount in the leachates is then measured by ICP-HR-MS, and by comparing the result with the maximum aluminum recovery extent in Table 4, we may calculate the aluminum recovery extent as shown in Table 5.

The corresponding residues of the leaching experiments in Table 5 were washed and analyzed by XRD, and then semi-quantitatively calculated as shown in Fig. 13. The co-existing phases of the obtained residues are relatively similar to the residues that are leached at 45 °C after 30 min in Fig. 8. However, semi-quantitative calculations of the fraction of the phases of the residues may indicate that the calcite most likely precipitates in the increasing order of CaO:Al_2O_3 mass ratio, which is seen in the residues of Slags 1, 2, and 3, and then it starts decreasing in residue of Slags 4 and 5. Vaterite, the less stable form of $CaCO_3$, precipitates only in the residue of Slags 1 and 2, while it is unobservable in the residues of Slags 3, 4, and 5. More details on the vaterite phase formation are discussed later.

A relatively high amount of bayerite (21–39 wt%) is detected in the residue of Slags 1 and 2, while a low trace of it is seen in the residue of Slag 4. We may say that the precipitation of bayerite gives a significant contribution to the low extent of aluminum recovery, especially for Slags 1 and 2, as it consumes three-quarter moles of CA phase for one mole of bayerite, as seen in reaction (12). Based on the semi-quantitative result in Fig. 13, we suggest that the aluminum recovery decreases by 0.4% for every percent of bayerite precipitation. Furthermore, the $Ca_3Al_2(OH)_{12}$ phase is noticed at relatively low quantities (< 6 wt%) in all of the residues. We may conclude that the extent of alumina recovery in leaching is affected by the unleached slags and precipitation of unwanted compounds as in reaction (12)–(14); $Ca_3Al_2(OH)_{12}$ and bayerite.

4.3. Leaching mechanism

As discussed in previous part, not all calcium aluminates have the same leaching behavior and extent as we would have expected in the equilibrium condition in Fig. 5. This means that thermodynamic consideration is not the only factor that defines the leachability of the calcium aluminate phases if a specific leaching rate is expected. In this section, we discuss other factors that may also contribute to the leaching property. Moreover, the changes in particles morphology before and after the leaching process are shown and discussed.

4.3.1. The structure of calcium-aluminate phases

The previously determined crystal structures of CA (Ma et al., 2011), CA_2 (Baldock et al., 1970), C_3A (Mondal and Jeffery, 1975), and $C_{12}A_7$ (Boysen et al., 2007) were observed in the current study. We model the atomic arrangements in a unit cell of calcium aluminates that is shown in Fig. 14. The drawings produced by VESTA™ ver.3, which is a program for three-dimensional visualization and investigation of crystal structures (Momma and Izumi, 2011).

The CA and CA_2 phase have monoclinic (Baldock et al., 1970; Ma et al., 2011), while C_3A and $C_{12}A_7$ phase have cubic lattice system (Boysen et al., 2007; Mondal and Jeffery, 1975). Ca- and Al-atom shares six (octahedral) and four (tetrahedral) coordination number with O-atom, respectively. Calcium aluminate slag is an ionic compound in nature; consists of cations, i.e., Ca^{2+} and Al^{3+}, and anions, i.e. O^- and O^{2-}. However, the Al-tetrahedral sites are joined together in chains by bridging oxygen (BO), this results in a polymerized network structure, which is considered as a network former. In other words, we could say that the slag consists of both covalent (joined tetrahedrons) and ionic (cation-oxygen) bonds. The strength of the cation-oxygen bond could be presented by the field strength (z/r^2), where z is the charge and r is the radius of the cation (Mills et al., 2013). From the formula, we may

Table 5
The pH of leachates and aluminum recovery in several leaching conditions.

Sample	Leaching condition			pH in the leachate	Aluminum in the leachate (g/L)	Aluminum recovery (%)
	Solution	Temperature (°C)	Time (minute)			
Slag 1	120 g/L	75	10	12.5 ± 0.1	3.1 ± 0.05	17.5 ± 0.3
Slag 2	Na_2CO_3	60	10	12.9 ± 0.1	4.0 ± 0.03	24.4 ± 0.2
Slag 3		45	10	12.9 ± 0.1	12.6 ± 0.03	93.3 ± 0.2
Slag 4		45	10	12.9 ± 0.1	6.1 ± 0.05	50.0 ± 0.4
Slag 5		45	10	12.8 ± 0.1	4.9 ± 0.14	46.2 ± 1.3

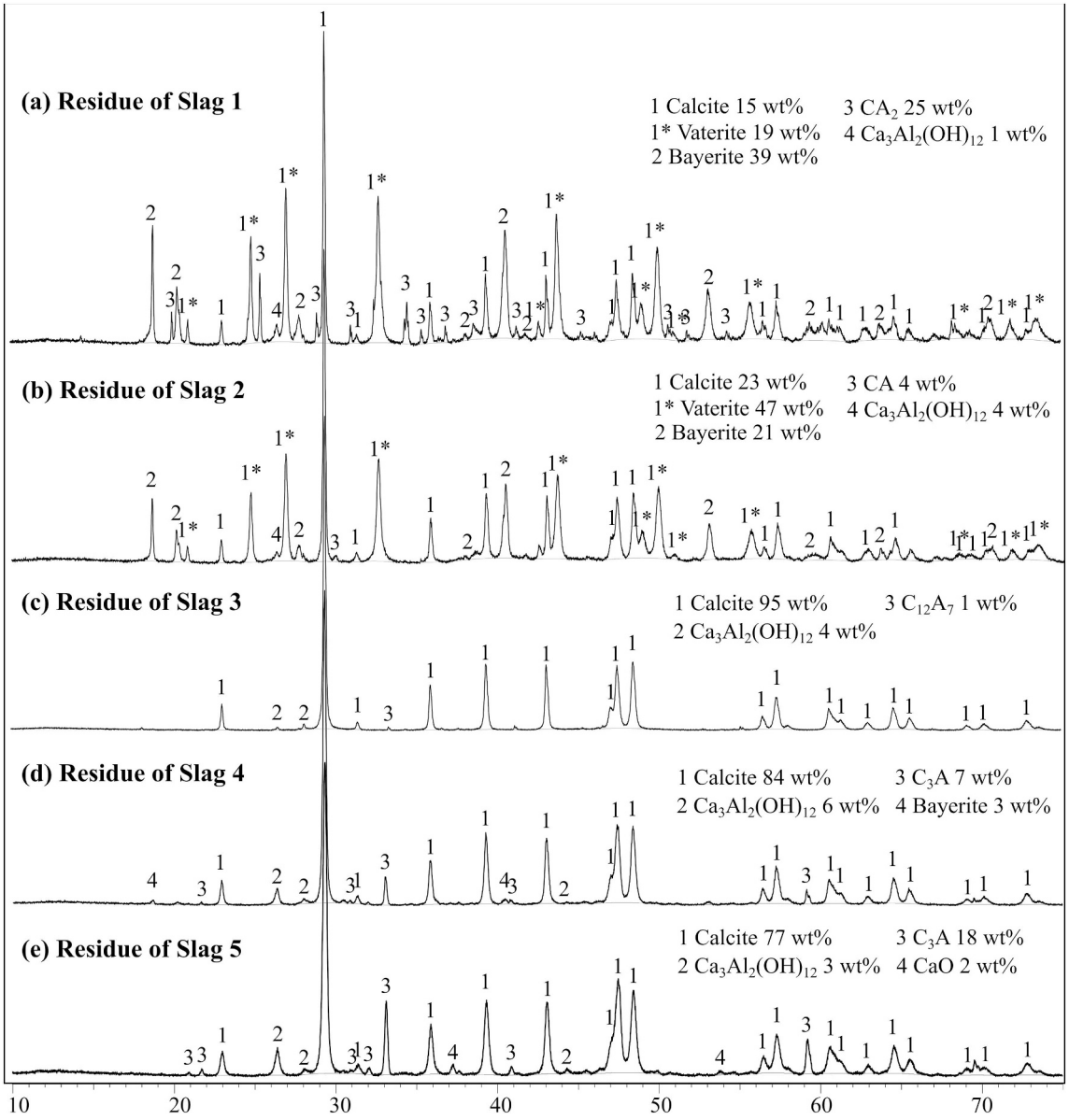

Fig. 13. XRD pattern of the obtained residues from the experiments carried out in conditions given in Table 5.

conclude that the field strength decreases with increasing cation size. Shannon (1976) stated that the Ca atomic radius is about two times larger than Al. Therefore, compared to the Al—O bond, the Ca—O bond is relatively weak.

Moreover, when Ca^{2+} and Na^{+} cations (in the form of Na_2O) co-exist in the structure, it tends to break the BO and form non-bridging oxygens (NBO). An NBO is oxygen that bridges from a tetrahedron to a neighboring, non-tetrahedral polyhedron (in this study, Ca-octahedral). The degree of polymerization of an aluminate compound is expressed as NBO/number of tetrahedral (T), whereas NBO/$T = 0$ shows a fully polymerized structure (Mysen, 1990; Mysen et al., 1985). In other words, by increasing the ratio of NBO/T then the structure is prone to depolymerize. Mills et al. (2013) proposed an equation of NBO/T as the ratio of the mole fraction of "available" network breaking oxides (where "available" means the total number of cations minus those on charge balancing duties) divided by the mole fraction of the network-forming oxides as in Eq. (18).

$$\mathrm{NBO/T} = 2(\sum X_{\mathrm{MO}} + \sum X_{\mathrm{M_2O}} - X_{\mathrm{Al_2O_3}})/(X_{\mathrm{SiO_2}} + 2X_{\mathrm{Al_2O_3}}) \quad (18)$$

Where X is the mole fraction and $X_{\mathrm{MO}} = X_{\mathrm{MgO}} + X_{\mathrm{CaO}} + X_{\mathrm{BaO}} + X_{\mathrm{FeO}} + X_{\mathrm{MnO}} + \ldots$ and $X_{\mathrm{M2O}} = X_{\mathrm{Li2O}} + X_{\mathrm{Na2O}} + X_{\mathrm{K2O}}$. The order of NBO/T for calcium aluminate phases in a typical leaching reaction (1)–(4) becomes $C_3A > C_{12}A_7 > CA > CA_2$. The index of the NBO/T of the Slags 1–5 and their leaching extent is shown in Table 6. It is noted here that the structure of $C_{12}A_7$ in Fig. 14 has a loose-bond of O-ions in the "cage," which may increase the depolymerize extent. Therefore, the NBO/T index for $C_{12}A_7$ becomes irrelevant. Nevertheless, the NBO/T order shows good agreement with the leachability of the calcium aluminate phases in literature (Azof et al., 2017; Fursman et al., 1968), where C_3A, $C_{12}A_7$, and CA are considered as the soluble phases in sodium carbonate solution, while CA_2 phase is the insoluble one. Also, Wells (1928) claimed that C_3A has a vigorous reaction towards the water, and the activity of the other aluminates (i.e., CA, C_5A_3) is distinctly less than that shown by C_3A. Thus it is obvious that the increasing degree of depolymerizing structure of calcium aluminates affecting the extent of its leaching property.

4.3.2. Morphology changes and size evolution

As mentioned in Section 4.2.1., the predominant phase of residue produced from the leaching reaction is $CaCO_3$. However, the formation

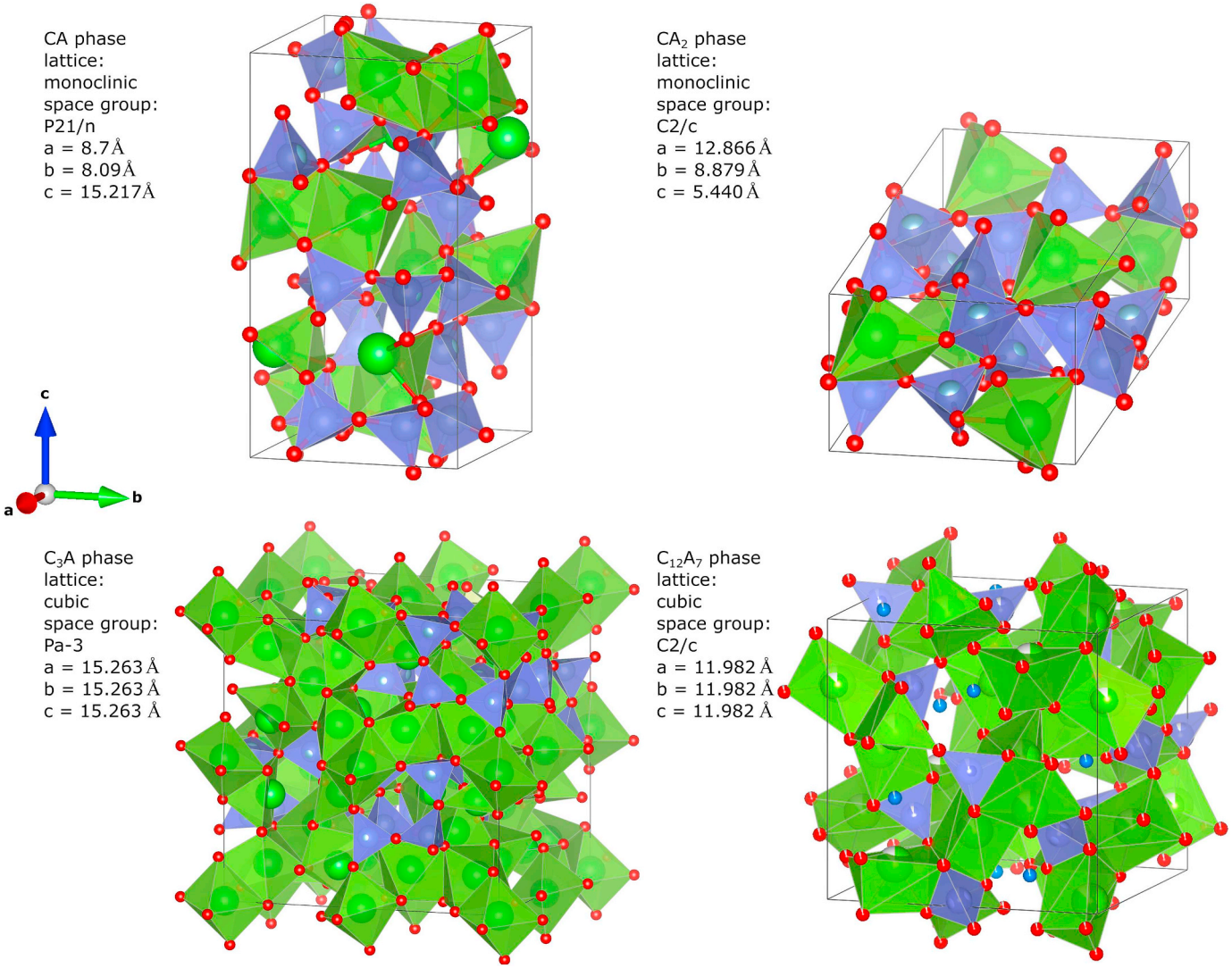

Fig. 14. Structure of CA, CA_2, C_3A, and $C_{12}A_7$ crystals. Green, light blue and red balls represent Ca, Al, and O atoms. AlO_4 tetrahedral and CaO_6 octahedral are shown by dark (purple) and light (green). The dark blue balls at the center of the $C_{12}A_7$ "cage" structure is the "free" O-ions in (1/4, 3/8, 0) position as proposed by Boysen et al. (2007). (For interpretation of the references to colour in this figure legend, the reader is referred to the web version of this article.)

Table 6
A relationship between NBO/T index of the slags and aluminum recovery.

Sample name	NBO/T index	Aluminum recovery* (%)
Slag 1	- 0.1	17.5 ± 0.3
Slag 2	0.1	24.4 ± 0.2
Slag 3**	N/A	93.3 ± 0.2
Slag 4	1.2	50.0 ± 0.4
Slag 5	1.4	46.2 ± 1.3

* Based on the ICP-HR-MS results in Table 5.

** Slag 3 consists of single $C_{12}A_7$ phase, which has "free" O-ions and easily depolymerize.

and morphology of residues produced from this typical reaction are still unclear. Fig. 15(a) shows the SEM image of solid Slag 1 before the leaching treatment, while Fig. 15(b), (c), and (d) show the residue with spherical and dendritic arm growth, agglomerated sphere particles with cauliflower-like in 3000×, and 5000× magnification, respectively. The SEM images of the residue are in agreement with the result of Hostomsky and Jones (1991) in their works on $CaCO_3$ precipitation from a supersaturated solution. They suggested that the agglomeration of an individual $CaCO_3$ particle is the dominant mechanism of increasing particle size compared to the primary crystal growth. This means that the agglomeration most likely causes changes in size.

Moreover, in Fig. 15(b) – (d) we see the morphology of the residue particles is in the small rounded particles clustered together, which is a typical morphology of vaterite (Söhnel and Mullin, 1982; Spanos and Koutsoukos, 1998). Vaterite is favorable to form at high pH (≥ 9.5) solution (Gómez-Morales et al., 1996; Hostomsky and Jones, 1991; Söhnel and Mullin, 1982). Also, vaterite is considered as a metastable phase and is gradually transformed into either calcite or aragonite, where calcite is the thermodynamically stable under normal conditions (Koutsoukos and Kontoyannis, 1984; Söhnel and Mullin, 1982). In the previous discussion in *4.2.4.*, and also shown in Fig. 13, the higher ratio of $CaO:Al_2O_3$ slags we have, the lower amount of vaterite would exist. However, it is difficult to distinguish the form of calcite and vaterite in Fig. 15 as it may not be separated clearly. Extensive works by Koutsoukos and Kontoyannis (1984) and Nancollas and Reddy (1971) showed that the temperature also plays an essential role in the precipitation rate of the vaterite's nuclei. However, it is relatively independent to the stirring speed (agitation).

According to the leaching mechanism that is discussed earlier in *4.3.1.*, depolymerization of solid calcium aluminates might take place in order to proceed with the leaching reactions. We suggest that the

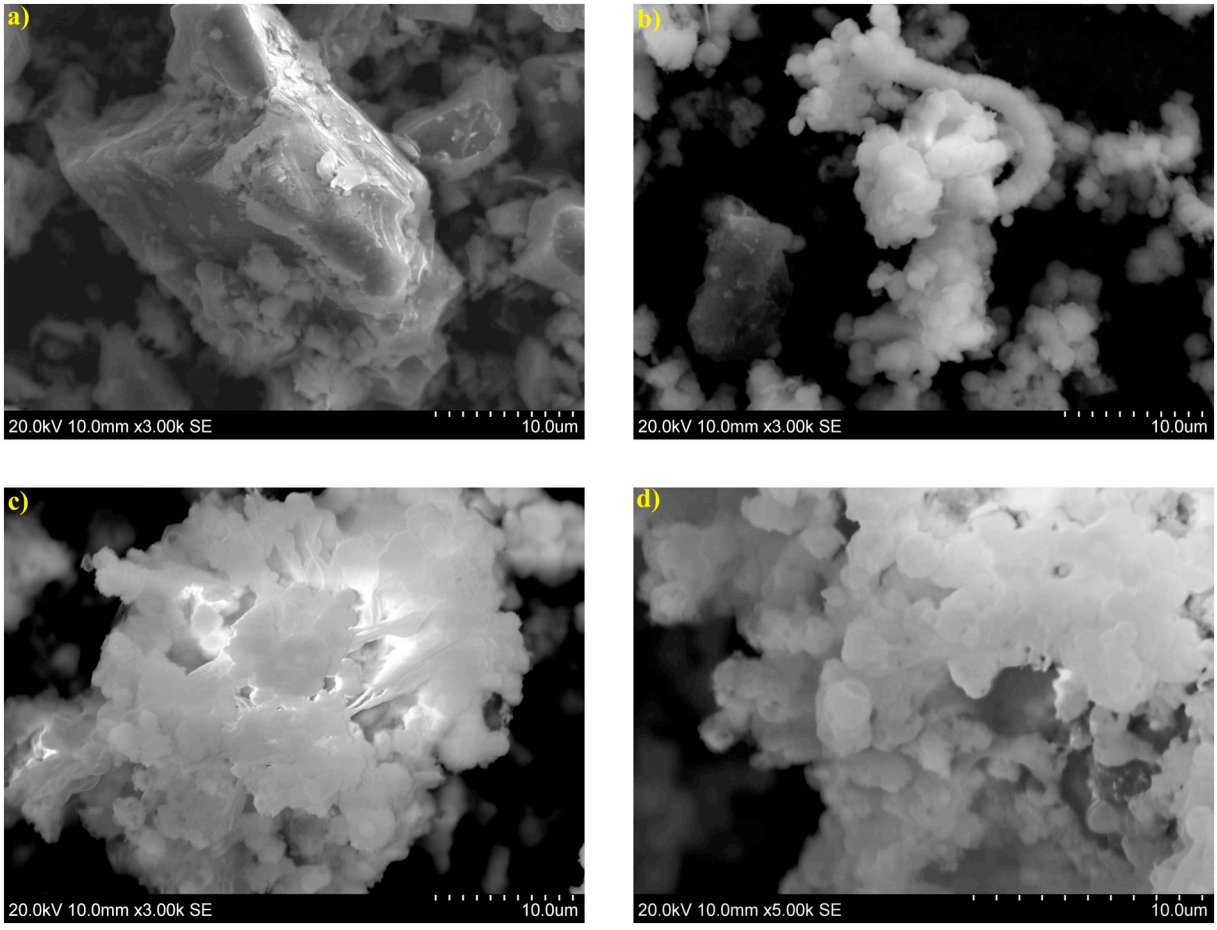

Fig. 15. SEM image of (a) the anisotropy and rock-like Slag 1, (b) spherical and dendritic arm growth of the residue, (c) and (d) agglomerated sphere particles with cauliflower-like in 3000× and 5000× magnification, respectively.

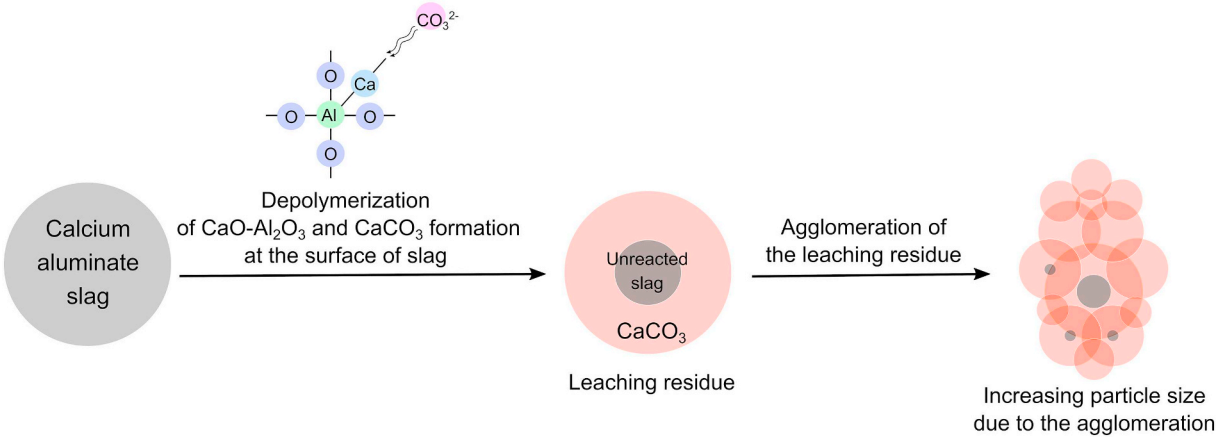

Fig. 16. Illustration of a leaching residue formation from a leachable calcium aluminate phase and increasing particle size of the $CaCO_3$-containing residue due to the agglomeration.

residue nucleation is taking place after the disintegration of solid slag in alkaline solution, which is caused by cations (Ca^{2+} and Na^{+}) depolymerization, and followed by strong ionic bonding between Ca^{2+}–CO_3^{2-}. In addition, we suggest that the primary nucleation is favorably taking place at the existing surface of particle (heterogeneous nucleation), in this case, the most suitable position is the surface of the reacting slag. Therefore, we may conclude here that the grown $CaCO_3$ layer at the surface of not completely reacted slag causes a slower conversion progress. Eventually, the more growth and then agglomeration of the $CaCO_3$-containing residue occur as illustrated in Fig. 16.

The evidence of agglomeration of $CaCO_3$-containing residue is shown by the particle size distribution of the obtained residue from Slags 1, 2, 3, and 4 in Fig. 17. It can be seen that the particle size could be classified into three different range; small (< 15 μm), moderate (30–40 μm), and large (100–170 μm). From Fig. 6 we know that the initial slags have an average of mean diameter < 15 μm. Considering

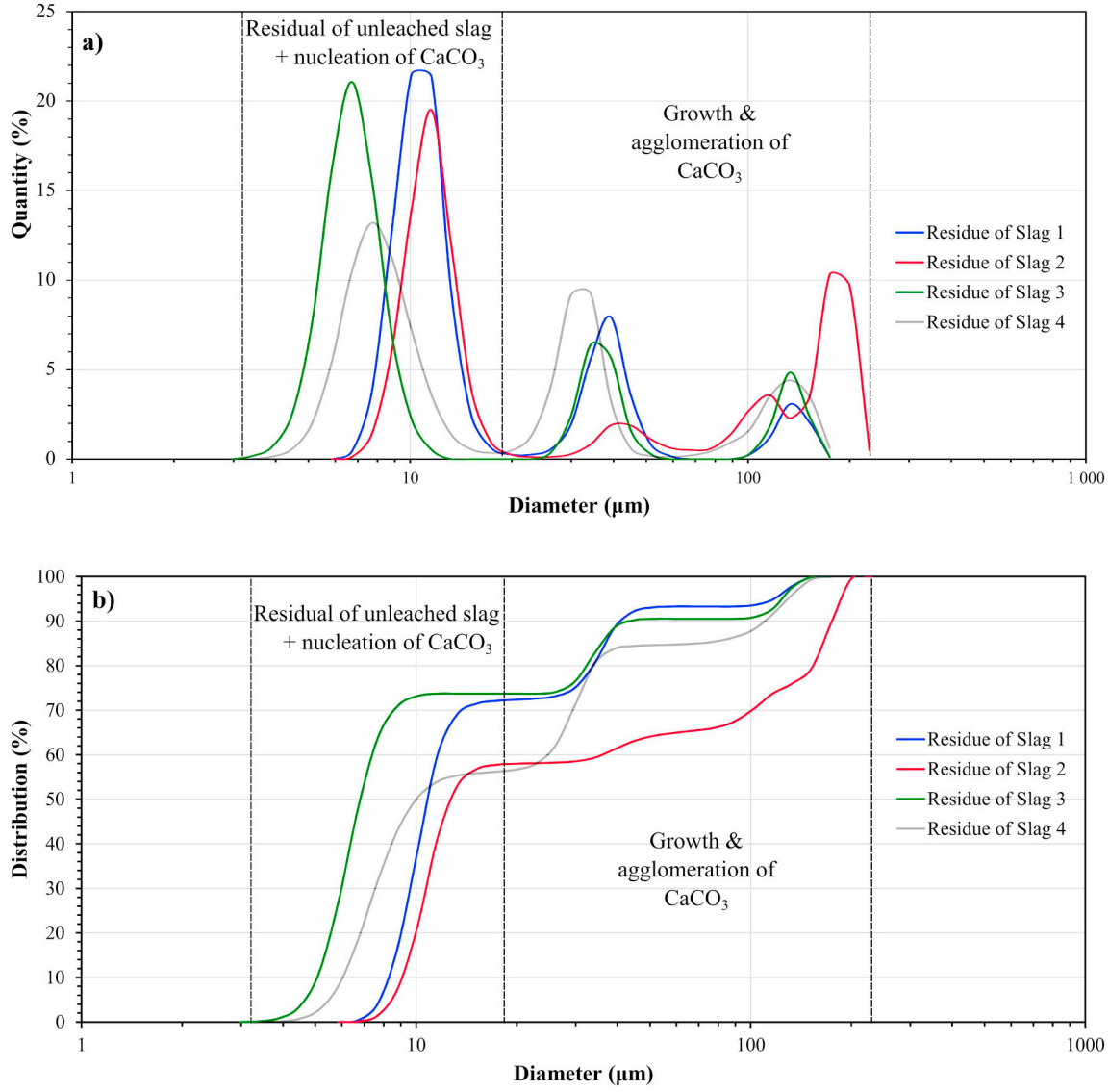

Fig. 17. Laser particle measurement based on (a) differential and (b) accumulative type of the obtained residues from Slags 1, 2, 3, and 4.

some slags were not reacted (or have low reactivity) with the Na_2CO_3 solution during the leaching treatment, the small range size of the residues is most likely a mixture of the residual of the unleached slag and primary nucleation of $CaCO_3$, while the moderate and large range sizes of the residues is composed mostly the $CaCO_3$ in vaterite and calcite forms. In general, the particle size range is relatively similar for all the obtained residues, which needs further investigation to see the factors that might influence the nucleation, growth, and agglomeration of the $CaCO_3$.

The use of the Scherrer equation (Langford and Wilson, 1978) to calculate the crystallite size through the full width at half maximum (FWHM) of each residue's XRD peak is not wise as the residue was finely grounded prior to the XRD observation, which, therefore, may give biased results on the precipitated and agglomerated residues.

The “humps” given by the laser particle measurement in Fig. 17(a) might give us doubt if the particle size was obtained without erroneous measures as the size classifications are so apparent and interestingly occur in each slag. Problems with the particle size measurement, in this case, employing laser diffraction, should be taken into account because the misrepresented data could lead us to an incorrect conclusion about the morphology and size evolution of the residues. Sabin (2011) described some issues related to the problems in measuring particle size employing the laser diffraction observation. Some of the problems are as follows:

(1) Broken particles that are caused by excessive ultrasonic energy,
(2) Bubble (artificial) peaks where the instrument cannot distinguish the particle and bubbles/gaseous objects, and.
(3) Opalescent/reflective particle artifact peaks where in some instances occurred when the particle is shiny, reflective, and opalescent.

Therefore, in an attempt to assure the results in Fig. 17, we have conducted SEM observation at low 100× and 500× magnification, which is shown in Fig. 18(a) and (b), respectively. By performing image analysis with ImageJ™, we can measure the size of the observed particles. Fine particle is excluded from the measurement as it is not easy to count small particles with an irregular shape. The result in Fig. 18(c) shows that the majority of coarse residues accounted for a moderate size diameter (30–40 µm), while the remainder is in tenth and hundredth-micrometer range, which support the measurement results in Fig. 17.

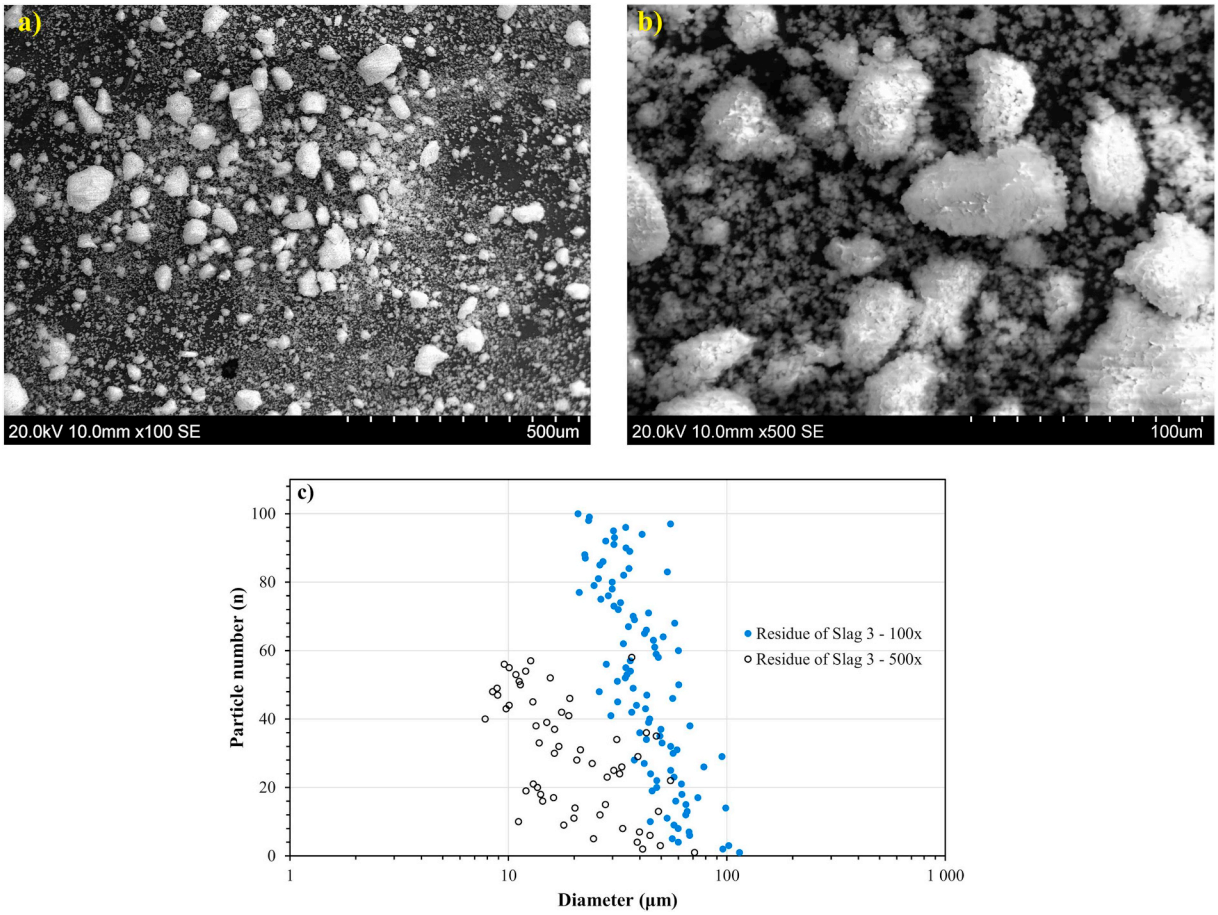

Fig. 18. SEM images of the residue of Slag 3 at (a) 100× and (b) 500× magnification, whereas, (c) the size distribution as calculated by ImageJ™ at coarse particles of $CaCO_3$ in (a) and (b).

5. Conclusions

A calcium aluminate slag which consists only $Ca_{12}Al_{14}O_{33}$ phase is seen as the most leachable slag in a sodium carbonate solution compared to the other slag compositions in the $CaO\text{-}Al_2O_3$ binary system. The leaching recovery may decrease with the precipitation of $Al(OH)_3$ in bayerite form, and $Ca_3Al_2(OH)_{12}$ phase. However, a "free-NaOH" can suppress the formation of those two compounds, accordingly. The less stable form of $CaCO_3$, vaterite, is likely formed in the residue from a relatively low calcium-containing slag (33–49 wt%), and the stable form, calcite, is optimally formed from slag which contains CaO > 49 wt%. The non-bridging oxygen (NBO) over tetrahedral structure (T) index shows that the atomic structure may affect the leaching extent of the slags, where in decreasing order the index of NBO/T of the calcium aluminate phases is $Ca_3Al_2O_6$ > $CaAl_2O_4$ > $CaAl_4O_7$. The $Ca_{12}Al_{14}O_{33}$ phase is an exception case where it has "free" O-ions at the center of the cage structure, which makes it easily depolymerize. The morphology and size changes of the obtained residues are apparent and clustered in the range of small (< 15 µm), moderate (30–40 µm), and large (100–170 µm), whereas the agglomeration of individual $CaCO_3$ particle might be the dominant mechanism of increasing particle size compared to the primary crystal growth.

Acknowledgement

Authors acknowledge Dr. Kai Tang (senior researcher at SINTEF Industry, Norway) for the contribution on the making of $CaO\text{-}Al_2O_3$ binary phase database in FactSage™ that includes $C_{12}Al_{14}O_{33}$ phase. The work was financed by NTNU [project number 237738], and supported by the Research Domain 5-Materials and Society in SFI Metal Production. The scientific support from ENSUREAL project (EU Horizon 2020) is also acknowledged.

References

Alekseev, A.I., 1982. Thermodynamic and experimental analysis of the system CaO-Al2O3-Na2O-H2O at 25-95 C. Zhurnal Prikl. Khimii 55, 2502–2506.
Alex, T.C., Kumar, R., Roy, S.K., Mehrotra, S.P., 2013. Leaching behaviour of high surface area synthetic Boehmite in NaOH solution. Hydrometallurgy. https://doi.org/10.1016/j.hydromet.2013.04.004.
Aluminum, World, 2015. Bauxite Residue Management: Best Practice.
Aruja, E., 1957. The unit cell of orthorhombic pentacalcium trialuminate, 5CaO.3Al203. Acta Crystallogr. 10, 337–339. https://doi.org/10.1107/S0365110X57000961.
Azof, F.I., Kolbeinsen, L., Safarian, J., 2017. The Leachability of calcium aluminate phases in slags for the extraction of alumina, in: Travaux 46. In: Proceedings of 35th International ICSOBA Conference. ICSOBA, Hamburg, pp. 243–253.
Azof, F.I., Kolbeinsen, L., Safarian, J., 2018a. Characteristics of calcium-aluminate slags and pig Iron produced from smelting-reduction of low-grade bauxites. Metall. Mater. Trans. B Process Metall. Mater. Process. Sci. 49, 2400–2420. https://doi.org/10.1007/s11663-018-1353-1.
Azof, F.I., Kolbeinsen, L., Safarian, J., 2018b. Characteristics of calcium-aluminate slags and pig Iron produced from smelting-reduction of low-grade bauxites. Metall. Mater. Trans. B Process Metall. Mater. Process. Sci. 49, 2400–2420. https://doi.org/10.1007/s11663-018-1353-1.
Baldock, P.J., Parker, A., Sladdin, I., 1970. X-ray powder diffraction data for calcium monoaluminate and calcium dialuminate. J. Appl. Crystallogr. 188–191.
Bayer, K.J., 1894. Process of Making Alumina. 515895.
Blake, H.E., Fursman, O.C., Fugate, A.D., Banning, L.H., 1966. Adaptation of the Pedersen process to the ferruginous bauxites of the Pacific Northwest. Bur. Mines US Dep. Inter. (6939), 1–21.
Bo, W., Hui-lan, S., Xue-zheng, Z., Shi-wen, B., 2011. The effect of cooling rate on the Leachability of calcium aluminate slags. In: Light Metals 2011. John Wiley & Sons, Inc., Hoboken, NJ, USA, pp. 241–244. https://doi.org/10.1002/9781118061992.ch43.

Bo, W., Jianxin, Z., Shufeng, Z., Huilan, S., 2014. Effect of Calcium/Aluminium Ratio on Crystal Structure and Al2O3 Leaching Property of 12CaO.7Al2O3. In: Light Metals 2014, pp. 87–90.
Bo, W., Jiajia, L., Huilan, S., Yubing, Z., Dongdong, L., 2015. Synergistic Effect of C12A7 and CA on Alumina Leaching Property under Low Calcium/Aluminum Ratio, in: Light Metals 2015. https://doi.org/10.1002/9781119093435.ch11.
Boysen, H., Lerch, M., Stys, A., Senyshyn, A., 2007. Structure and oxygen mobility in mayenite (Ca12Al14O33): a high-temperature neutron powder diffraction study. Acta Crystallogr. Sect. B Struct. Sci. 63, 675–682. https://doi.org/10.1107/S0108768107030005.
Brisi, C., Borlera, M.L., Montanaro, L., Negro, A., 1986. Hydration of 5CaO.3Al2O3. Cem. Concr. Res. 16, 156–160.
Büssem, W., 1936. Die Struktur des Pentacalciumtrialuminats. Zeitschrift für Krist. - Cryst. Mater. 95. https://doi.org/10.1524/zkri.1936.95.1.175.
Chipera, S.J., Bish, D.L., 2013. Fitting full X-ray diffraction patterns for quantitative analysis: a method for readily quantifying crystalline and disordered phases. Adv. Mater. Phys. Chem. 03, 47–53. https://doi.org/10.4236/ampc.2013.31A007.
Dentoni, V., Grosso, B., Massacci, G., 2014. Environmental sustainability of the alumina industry in Western Europe. Sustain. 6. https://doi.org/10.3390/su6129477.
Fursman, O.C., Blake Jr., H.E., Mauser, J.E., 1968. Recovery of Alumina and Iron from Pacific Northwest Bauxites by the Pedersen Process. Albany.
Gómez-Morales, J., Torrent-Burgués, J., Rodríguez-Clemente, R., 1996. Nucleation of calcium carbonate at different initial pH conditions. J. Cryst. Growth 169, 331–338. https://doi.org/10.1016/S0022-0248(96)00381-8.
Gu, Songqing, Qi, Lijuan, Zhonglin, Y., 2007. Energy Consumption in Bayer Process, in: Light Metals 2007. pp. 55–59.
Guirado, F., Galí, S., Chinchón, S., 2000. Quantitative Rietveld analysis of aluminous cement clinker phases. Cem. Concr. Res. 30, 1023–1029. https://doi.org/10.1016/S0008-8846(00)00289-1.
Haccuria, E., Crivits, T., Hayes, P.C., Jak, E., 2016. Selected phase Equilibria studies in the Al2O3-CaO-SiO2 system. J. Am. Ceram. Soc. 99, 691–704. https://doi.org/10.1111/jace.13991.
Hallstedt, B., 1990. Assessment of the CaO-Al2O3 system. J. Am. Ceram. Soc. 73, 15–23.
Hayashi, K., Hirano, M., Matsuishi, S., Hosono, H., 2002. Microporous crystal 12CaO·7Al 2 O 3 encaging abundant O - radicals. J. Am. Chem. Soc. 124, 738–739. https://doi.org/10.1021/ja016112n.
Hostomsky, J., Jones, A.G., 1991. Calcium carbonate crystallization, agglomeration and form during continuous precipitation from solution. J. Phys. D. Appl. Phys. 24, 165–170. https://doi.org/10.1088/0022-3727/24/2/012.
Imlach, J.A., Glasser, L.S.D., Glasser, F.P., 1971. Excess oxygen and the stability of 12CaO.7Al2O3. Cem. Concr. Res. (1), 57–61.
Jeevaratnam, J., Glasser, F.P., Glasser, L.S.D., 1964. Anion substitution and structure of 12CaO.7Al2O3. J. Am. Ceram. Soc. 47, 105–106. https://doi.org/10.1111/j.1151-2916.1964.tb15669.x.
Jerebtsov, D., Mikhailov, G., 2001. Phase diagram of CaO–Al2O3 system. Ceram. Int. 27, 25–28. https://doi.org/10.1016/S0272-8842(00)00037-7.
Koutsoukos, P.G., Kontoyannis, C.G., 1984. Precipitation of calcium carbonate in aqueous solutions. J. Chem. Soc. Faraday Trans. 1 Phys. Chem. Condens. Phases 80, 1181. https://doi.org/10.1039/f19848001181.
Langford, J.I., Wilson, A.J.C., 1978. Scherrer after sixty years: a survey and some new results in the determination of crystallite size. J. Appl. Crystallogr. 11, 102–113. https://doi.org/10.1107/S0021889878012844.
Lundquist, R.V., Leitch, H., 1963a. Solubility characteristics of monocalcium aluminate. US Dept. Inter. Bur. Mines 6294, 1–9.
Lundquist, R.V., Leitch, H., 1963b. Two Hydrated Calcium Aluminates Encountered in the Lime-Soda Sinter Process. US Dept. Inter. Bur. Mines, pp. 6335.
Lundquist, R.V., Leitch, H., 1964. Aluminum Extraction Characteristics of Three Calcium Aluminates in Water, Sodium Hydroxide, and Sodium Carbonate Solutions. Bureau of Mines, Boulder City.
Lutsyk, V.I., Zelenaya, A.E., Savinov, V.V., 2012. Phase trajectories in CaO-Al2O3-SiO2 melts. Crystallogr. Reports 57, 943–947. https://doi.org/10.1134/S1063774512070176.
Ma, C., Kampf, A.R., Connolly, H.C., Beckett, J.R., Rossman, G.R., Smith, S.A.S., Schrader, D.L., 2011. Krotite, CaAl2O4, a new refractory mineral from the NWA 1934 meteorite. Am. Mineral. 96, 709–715. https://doi.org/10.2138/am.2011.3693.
Mach, T., 2012. Energy Consumption in the Bayer Process. In: International Alumina Quality Workshop, pp. 375–378.
Mao, H., Hillert, M., Selleby, M., Sundman, B., 2006. Thermodynamic assessment of the CaO-Al2O3-SiO2 system. J. Am. Ceram. Soc. 89, 298–308. https://doi.org/10.1111/j.1551-2916.2005.00698.x.
Meyer, F.M., 2004. Availability of bauxite reserves. Nat. Resour. Res. 13, 161–172. https://doi.org/10.1023/B:NARR.0000046918.50121.2e.
Mills, K.C., Hayashi, M., Wang, L., Watanabe, T., 2013. The structure and properties of silicate slags. Treatise on Process Metallurgy. Elsevier Ltd. https://doi.org/10.1016/B978-0-08-096986-2.00008-4.
Momma, K., Izumi, F., 2011. VESTA 3 for three-dimensional visualization of crystal, volumetric and morphology data. J. Appl. Crystallogr. 44, 1272–1276. https://doi.org/10.1107/S0021889811038970.
Mondal, P., Jeffery, J.W., 1975. The crystal structure of tricalcium aluminate, Ca3Al2O6. Acta Crystallogr. B 31, 689–697. https://doi.org/10.1107/S0567740875003639.
Moolenaar, R.J., Evans, J.C., McKeever, L.D., 1970. The structure of the aluminate ion in solutions at high pH. J. Phys. Chem. 74, 3629–3636. https://doi.org/10.1021/j100714a014.
Mysen, B.O., 1990. Relationships between silicate melt structure and petrologic processes. Earth Sci. Rev. 27, 281–365. https://doi.org/10.1016/0012-8252(90)90055-Z.
Mysen, B.O., Virgo, D., Seifert, F.A., 1985. Relationships between properties and structure of aluminosilicate melts. Am. Mineral. 70, 88–105. https://doi.org/10.1007/BF00413348.
Nancollas, G., Reddy, M., 1971. The crystallization of calcium carbonate. II. Calcite growth mechanism. J. Colloid Interface Sci. 37, 824–830. https://doi.org/10.1016/0021-9797(71)90363-8.
Nurse, R.W., Welch, J.H., Majumdar, A.J., 1965a. The CaO-Al2O3 system in a moisture-free atmosphere. Trans. Br. Ceram. Soc. 64, 409–418.
Nurse, R.W., Welch, J.H., Majumdar, A.J., 1965b. The 12CaO.7Al2O3 Phase in the CaO-Al2O3 System. Trans. Br. Ceram. Soc 64, 323–332.
Pedersen, H., 1927. Process of Manufacturing Aluminum Hydroxide. 1618105.
Pitzer, K.S., 1973. Thermodynamics of electrolytes. I. Theoretical basis and general equations. J. Phys. Chem. 77, 268–277. https://doi.org/10.1021/j100621a026.
Rankin, G.A., Wright, F.E., 1915. The ternary system CaO-Al2O3-SiO2. Am. J. Sci. 39.
Roy, D.M., Roy, R., 1960. Crystalline solubility and zeolitic behavior in garnet phases in the system CaO-Al2O3-SiO2-H2O. In: Fourth international symposium on the chemistry of cement. Washington D.C, pp. 307–314.
Sabin, A., 2011. Problems in particle size: laser diffraction observations. Fine Part. Tecnol. 15, 35–43.
Safarian, J., 2018. Extraction of Iron and Ferrosilicon Alloys from Low-Grade Bauxite Ores, in: Extraction 2018, the Minerals. Metals & Materials Series. Springer International Publishing, Cham, pp. 825–837. https://doi.org/10.1007/978-3-319-95022-8_66.
Safarian, J., Kolbeinsen, L., 2016a. Sustainability in Alumina Production from Bauxite. In: Sustainable Industrial Processing Summit, pp. 75–82.
Safarian, J., Kolbeinsen, L., 2016b. Smelting-reduction of Bauxite for Sustainable Alumina Production. In: Sustainable Industrial Processing Summit, pp. 149–158.
Sellaeg, H., Kolbeinsen, L., Safarian, J., 2017. Iron Separation from Bauxite Through Smelting-Reduction Process. In: Minerals, Metals and Materials Series, pp. 127–135. https://doi.org/10.1007/978-3-319-51541-0_19.
Shannon, R.D., 1976. Revised effective ionic radii and systematic studies of interatomic distances in halides and chalcogenides. Acta Crystallogr. Sect. A 32, 751–767. https://doi.org/10.1107/S0567739476001551.
Shepherd, E.S., Rankin, G.A., Wrigth, F.E., 1909. The binary Systems of Alumina with silica, lime and magnesia.Pdf. Am. J. Sci. 28, 293–333.
Smith, P., 2009. The processing of high silica bauxites - review of existing and potential processes. Hydrometallurgy. https://doi.org/10.1016/j.hydromet.2009.04.015.
Söhnel, O., Mullin, J.W., 1982. Precipitation of calcium carbonate. J. Cryst. Growth 60, 239–250. https://doi.org/10.1016/0022-0248(82)90095-1.
Spanos, N., Koutsoukos, P.G., 1998. Kinetics of precipitation of calcium carbonate in alkaline pH at constant Supersaturation. Spontaneous and seeded growth. J. Phys. Chem. B 102, 6679–6684. https://doi.org/10.1021/jp981171h.
Sun, H., Wang, B., Yu, H., Bi, S., Tu, G.-F., 2010. Effect of Na2O on Alumina Leaching and Self-Disintegrating Property of Calcium Aluminate Slag. In: Light Metals 2010.
Sun, H.L., Wang, B., Zhang, J.X., Zong, S.F., 2014. Characterization and alumina leachability of 12CaO·7Al2O3 with different holding times. Adv. Mater. Sci. Eng. https://doi.org/10.1155/2014/730616.
Thorvaldson, T., Schneider, W.G., 1941. The composition of the “5:3” calcium aluminate. Can. J. Res. 19b, 109–115. https://doi.org/10.1139/cjr41b-015.
Wells, L.S., 1928. Reaction of water on calcium aluminates. Bur. Stand. J. Res. 1, 951. https://doi.org/10.6028/jres.001.034.
Whittington, B.I., Cardile, C.M., 1996. The chemistry of tricalcium aluminate hexahydrate relating to the Bayer industry. Int. J. Miner. Process. 48, 21–38. https://doi.org/10.1016/S0301-7516(96)00011-7.
Whittington, B.I., Fallows, T.M., Willing, M.J., 1997. Tricalcium aluminate hexahydrate (TCA) filter aid in the Bayer industry: factors affecting TCA preparation and morphology. Int. J. Miner. Process. 49, 1–29. https://doi.org/10.1016/S0301-7516(96)00035-X.
Yu, H., Pan, X., Wang, B., Zhang, W., Sun, H., Bi, S., 2012. Effect of Na2O on formation of calcium aluminates in CaO–Al2O3–SiO2 system. Trans. Nonferrous Met. Soc. China 22, 3108–3112. https://doi.org/10.1016/S1003-6326(11)61578-1.
Zhang, Y., Lü, W., Qi, Y., Zou, Z., 2016. Recovery of iron and calcium aluminate slag from high-ferrous bauxite by high-temperature reduction and smelting process. Int. J. Miner. Metall. Mater. 23, 881–890. https://doi.org/10.1007/s12613-016-1303-3.
Zhmoidin, G.I., Chatterjee, A.K., 1984. Conditions and mechanism of Interconvertibility of compounds 12CaO.7Al2O3 and 5CaO.3Al2O3. Cem. Concr. Res. 14, 386–396. https://doi.org/10.1016/0008-8846(84)90057-7.
Zhou, Y., Wu, L., Wang, J., Wang, H., Dong, Y., 2013. Alumina extraction from high-alumina ladle furnace refining slag. Hydrometallurgy. https://doi.org/10.1016/j.hydromet.2013.08.007.